Helical phases assembled from achiral molecules: twist-bend nematic and helical filamentary B_4 phases formed by mesogenic dimers.

CRUICKSHANK, E., ANDERSON, K., STOREY, J.M.D., IMRIE, C.T., GORECKA, E., POCIECHA, D., MAKAL, A. and MAJEWSKA, M.M.

2022

Journal of Molecular Liquids 346 (2022) 118180

Contents lists available at ScienceDirect

Journal of Molecular Liquids

journal homepage: www.elsevier.com/locate/molliq

Helical phases assembled from achiral molecules: Twist-bend nematic and helical filamentary B_4 phases formed by mesogenic dimers

E. Cruickshank [a], K. Anderson [a], J.M.D. Storey [a], C.T. Imrie [a], E. Gorecka [b], D. Pociecha [b], A. Makal [b], M.M. Majewska [b,*]

[a] Department of Chemistry, School of Natural and Computing Sciences, University of Aberdeen, Meston Building, Aberdeen AB24 3UE, UK
[b] Faculty of Chemistry, University of Warsaw, ul. Zwirki i Wigury 101, 02-089 Warsaw, Poland

ARTICLE INFO

Article history:
Received 10 September 2021
Revised 19 November 2021
Accepted 21 November 2021
Available online 26 November 2021

Keywords:
Liquid crystals
Nematic phase
Helical nanofilament
B4 phase

ABSTRACT

The synthesis and characterisation of an homologous series of bent odd-membered mesogenic dimers, the 4′-(6-{4-[(E)-{[4-(alkylthio)phenyl]imino}-methyl]phenoxy}hexyl)[1,1′-biphenyl]-4-carbonitriles (CB6O.S*m*) is reported. This general class of materials, despite being achiral, has a strong tendency to form helical structures, and here, for the first time we report three such chiral phases in a single homologous series. Specifically, the heliconical twist-bend nematic (N_{TB}) phase for short terminal thioalkyl chains, and its smectic equivalent - the twist-bend smectic C (SmC_{TB}) phase for longer chains. All the dimers showed the helical filament B_4 phase, which is typically seen for rigid bent-core mesogens, but has only rarely been reported for flexible dimeric molecules. In addition, on increasing chain length, smectic behaviour emerges including the smectic A and the smectic C_{TB} phases. We also show that these materials have the potential for their morphology to be controlled through surface interactions. The presence of the little-studied thio-linkage in the terminal chain, and the wide range of properties present in this single group of homologues, with promise of broad applicability in optics, photonics, as well as fundamental significance as a case study to achieve a better understanding of chirality and symmetry breaking in liquid crystals, ensures the importance of this new series of mesogens.

1. Introduction

How chirality originates in the absence of a chiral inductor is amongst the most important and topical of scientific questions, cutting across all disciplines, and having clear fundamental and technological relevance (see for example [1]). In this context, liquid crystals provide a wonderful test-bed for studying spontaneous mirror symmetry breaking in fluids [2]. Indeed, the first example of spontaneous mirror symmetry breaking in a fluid with no spatial ordering was the twist-bend nematic, N_{TB}, phase [3–6]. In a conventional nematic phase, the molecules all tend to align in the same direction, known as the director, whereas their centers of mass are randomly distributed. In the N_{TB} phase, the director forms a helix and is tilted with respect to the helical axis (a heliconical structure); the pitch length of the helix is very short, typically ~10 nm. *i.e.* just a few molecular lengths. The formation of chirality is spontaneous and so equal numbers of left- and right-handed helices are expected and overall, the system is racemic. This degeneracy may be removed by the introduction of intrinsic molecular chirality, leading to the N_{TB}^* phase [7]. The vast majority of materials that show the N_{TB} phase may be described as odd-membered dimers, in which two mesogenic units are attached by a flexible spacer containing an odd number of atoms, and such molecules have a bent molecular shape [8–11], however this phase has also been observed for rigid bent-core mesogens [12] as well as for oligomers including both, linear and bent-core segments [13]. Recently it was shown that odd-membered dimers not only exhibit the N_{TB} phase but also show twist-bend smectic phases [14–17]. In these fascinating heliconical lamellar phases consisting of achiral molecules up to four levels of structural chirality were observed: layer chirality, helicity of a basic repeating unit, a mesoscopic helix and helical filaments. Another phase with a spontaneously chiral structure built of achiral molecules is the helical nanofilament phase (HNF, B_4), most commonly observed for rigid bent core mesogens [18,19] and only rarely for bent dimers [20].

In our search for new examples of chiral systems made of achiral building blocks, here we report the synthesis and characterization of non-symmetric dimeric mesogens consisting of a cyanobiphenyl core, an odd-membered spacer and a benzylidene

* Corresponding author.
E-mail address: mmajewska@chem.uw.edu.pl (M.M. Majewska).

https://doi.org/10.1016/j.molliq.2021.118180
0167-7322/

aniline unit terminated with an alkylthio chain, the 4′-(6-{4-[(E)-{[4-(alkylthio)phenyl]imino}-methyl]phenoxy}hexyl)[1,1′-biphenyl]-4-carbonitriles (Fig. 1) and refer to them using the acronym CB6O.S*m*, in which *m* denotes the number of carbon atoms in the terminal chain. The flexible hexyloxy spacer linking the two mesogenic units contains seven atoms, and ensures the necessary molecular curvature required for twist-bend phases to be observed [21,22]. Liquid crystals with terminal alkylthio chains are extremely topical due to their high values of birefringence arising from the polarisable sulfur atom [23–25]. Highly birefringent nematogens have the potential not only to improve liquid crystal display technology, but also have an important role to play in emerging fields such as liquid crystal lasers and lenses [26,27]. Fundamentally, the introduction of the thio linkage is providing a demanding challenge to our understanding of the relationships between molecular structure and liquid crystalline behaviour [28–31].

The CB6O.S*m* series exhibits a rich range of phase behaviour depending on the length of the terminal chain including twist-bend phases, and the B_4 phase [18,19] at room temperature, a crystalline phase with an unusual morphology of twisted filaments. The properties of the CB6O.S*m* series are compared to those of the analogous materials having alkyl CB6O.*m* [32] and alkyloxy CB6O.O*m* [33] terminal chains.

2. Experimental section

2.1. Synthesis

The synthetic route used to prepare the CB6O.S*m* series is shown in Scheme SI1 in the ESI along with detailed descriptions of their synthesis, including the structural characterization data for all intermediate and final products.

2.2. Methods

The phase behaviour of the CB6O.S*m* series was studied by differential scanning calorimetry (DSC) using a Mettler Toledo DSC1 calorimeter equipped with a TSO 801RO sample robot and calibrated using indium and zinc standards. The optical studies of the phases were conducted using a Zeiss Axio Imager A2m polarised light microscope with a Linkam heating stage. The samples were placed either between two untreated thin glass slides or in glass cells with planar anchoring induced by a thin inner layer of polymer. The cells were filled by capillary action with the material in the isotropic phase. Birefringence was measured using a setup based on a photoelastic modulator (PEM-90, Hinds) working at a modulation $f = 50$kHz; as a light source a halogen lamp (Hamamatsu LC8) was used, equipped with a narrow band pass filter (532 nm). The transmitted light intensity was measured with a photodiode (FLC Electronics PIN-20) and deconvoluted with a lock-in amplifier (EG&G 7265) into 1*f* and 2*f* components to yield a retardation induced by the sample. The dielectric permittivity was measured using a Wayne Kerr Precision Component Analyzer 6425, at the frequency 12 kHz, and with the applied voltage amplitude (V) ranging from 0.1 to 5.0 V. The splay elastic constant K_{11} was determined from the threshold voltage V_{th} at which the director reorientation starts, and thus the effective permittivity (ε) starts to grow as:$K_{11} = \Delta\varepsilon\varepsilon_0\left(\frac{V_{th}^2}{\pi^2}\right)$. The bend elastic constant, K_{33} was estimated by fitting the $\varepsilon(V)$ dependence far above the threshold voltage using [34]:

$$\frac{\varepsilon(V)-\varepsilon_\perp}{\varepsilon_{II}-\varepsilon_\perp} = 1 - \frac{2}{\pi}\sqrt{1+\xi}\frac{V_{th}}{V}\int_0^1 \sqrt{\frac{1+\kappa x^2}{1+\xi x^2}}dx$$

where $\xi = \frac{\varepsilon_{II}-\varepsilon_\perp}{\varepsilon_\perp}$ and $\kappa = \frac{K_{33}-K_{11}}{K_{11}}$.

For X-ray measurements three different set-ups were used, the Bruker D8 Discover, Bruker GADDS and Bruker Nanostar systems, all using CuKα radiation, λ = 1.54 Å. The samples for these measurements were prepared in the form of a thin film or a droplet on a heated surface. For AFM measurements, a Bruker Dimension Icon Microscope was used in tapping or scan assist mode. The cantilevers with elastic constant of 0.4 N/cm^2 were applied. The SEM measurements were performed using a FE-SEM Zeiss Merlin electron microscope operating at 5 keV utilizing an in-lens detector of secondary electrons. Samples were sputter coated with gold and palladium before imaging. To align the B_4 phase, the material was filled into porous anodic aluminium oxide (AAO) with a 60 nm pore size provided by Prof. Dong Ki Yoon's group from the Korea Advanced Institute of Science and Technology; the nanoconfinement prompted the formation of highly ordered nanostructures [35]. The CD spectra were recorded using a Chirascan Plus Applied Photophysics spectrometer. Samples with large domains of B_4 crystals were grown by placing material on a quartz slide, heating it to the isotropic liquid and cooling to room temperature.

3. Results and discussion

The phase transition temperatures and associated scaled entropy changes for the CB6O.S*m* series are given in Table S1 in ESI. The dependence of the transition temperatures on the length of the terminal alkylthio chain *m* is shown in Fig. 2. The homologues with *m* = 1–11 show the conventional nematic phase and, the twist-bend nematic phase below, apart from compounds *m* = 9 and *m* = 10, the observed mesophases are monotropic. For CB6O.S3 crystallization precluded the observation of the N_{TB} phase, and a virtual N-N_{TB} transition temperature was estimated from a phase diagram constructed using binary mixtures of CB6O.S3 and CB7CB [6]. The longer homologues, $m \geq 12$, showed smectic phases below the nematic phase.

The N - N_{TB} phase transition was accompanied by the appearance of the characteristic stripe texture (Fig. 3(a) and (b)), that is formed due to the pseudo-layer undulation in a confined cell

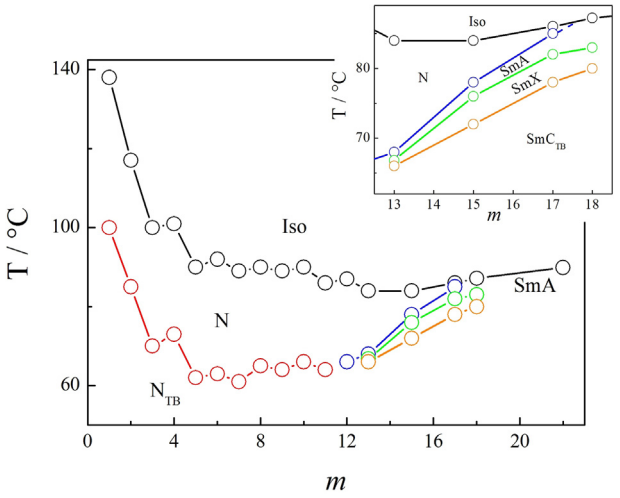

Fig. 2. The dependence of the transition temperatures on the length of the terminal alkylthio chain, *m*, for the CB6O.S*m* series, the temperatures were registered on cooling. The inset shows an expanded region of the phase diagram for *m* = 13–18.

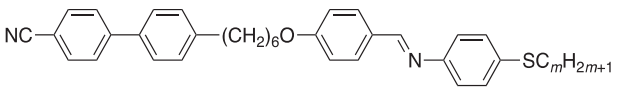

Fig. 1. Chemical structure of the CB6O.S*m* series, *m* = 1–13, 15, 17, 18, 22.

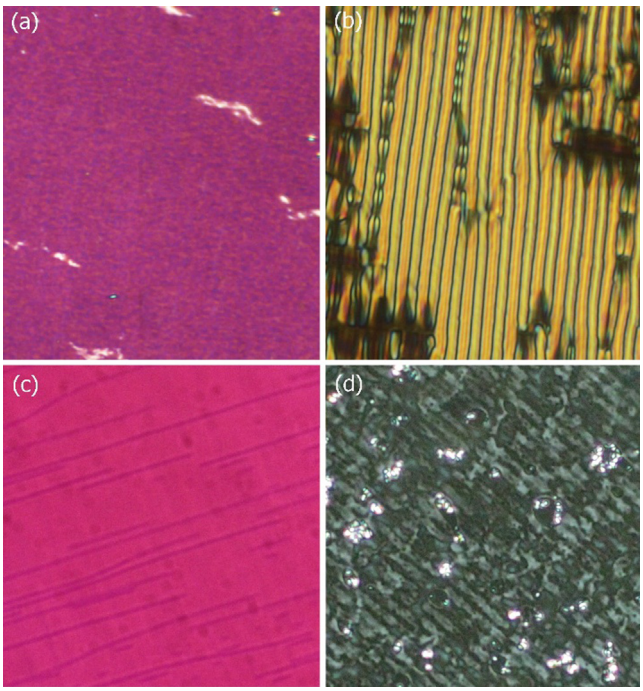

Fig. 3. Optical textures of the (a) N phase and (b) N_{TB} phase for CB6O.S9 observed in a 1.6-μm thick planar cell. Textures of the SmX phase for CB6O.S18 observed in (c) a 1.6-μm thick planar cell and (d) a cell with homeotropic anchoring. In an homeotropic cell the SmX phase forms a texture with a regular array of stripes. Thin darker lines visible in panel (c) are the regions of slightly higher birefringence.

geometry [36]. The X-ray patterns of the nematic and twist-bend nematic phases are almost indistinguishable. In the low diffraction angle range, despite the presence of the heavy sulfur atom in the molecular structure, there are broad signals of very weak intensity as also seen for the corresponding dimers having alkyloxy terminal chains, the CB6O.O*m* series [33]. For the short homologues, the low angle diffraction signal corresponds to half the molecular length, and on increasing the terminal chain length a signal related to the full molecular length appears and grows in intensity (Fig. 4). For the longest homologues, the X-ray diffraction pattern of the nematic phase contains a signal corresponding to twice the molecular length, which on cooling narrows and becomes apparatus-resolution limited in the smectic phase. This indicates that the smectic phases have a repeating structural unit composed of a molecular bilayer.

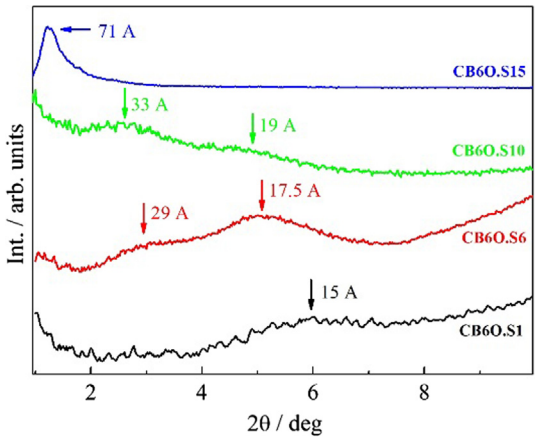

Fig. 4. Low angle X-ray diffraction patterns recorded in the nematic phase of CB6O.S*m* homologues with different lengths of terminal chain. Real space distances corresponding to the signal positions are indicated.

Formation of the N_{TB} phase, in which the molecules are tilted with respect to the helical axis, is accompanied by a deviation of the optical birefringence, Δn, from its power law temperature dependence observed in the nematic phase (Fig. 5). By analyzing the Δn decrease, the conical angle in the twist-bend nematic phase was determined according to the procedure described by Meyer et al. [37] to be ~20 deg. far from the N-N_{TB} transition. Interestingly, the measured optical birefringence starts to deviate from the power law dependence several degrees above the N-N_{TB} transition temperature, and this has been attributed to pretransitional fluctuations, specifically the formation of an instantaneous heliconical structure in the N phase [38].

The value of the optical birefringence expected for the nematic phase with ideal orientational order, S = 1, Δn_{max}, decreases on increasing the length of the terminal chain; for CB6O.S9 $\Delta n_{max} = 0.355$ and for CB6O.S17, $\Delta n_{max} = 0.302$. This decrease may be attributed to the reduction in the polarizability anisotropy of the molecule on changing the ratio between the strongly anisotropic mesogenic cores and the less anisotropic alkyl chains. The static dielectric anisotropy, $\Delta\varepsilon$, in the nematic phase is small and positive (Fig. S8). This implies that the dimers are locally arranged head-to-head, such that the longitudinal dipole moments associated with the cyano groups are almost compensated. The bend elastic constant is smaller than the splay elastic constant, $K_{33} < K_{11}$, over almost the entire temperature range of the nematic phase (Fig. S8), and this is typical behavior for bent dimers [34]. K_{33} decreases strongly upon approaching the twist-bend nematic phase whereas K_{11} increases monotonically with decreasing temperature and increasing order parameter.

For the longer homologues, a smectic A phase was formed on cooling the nematic phase (m = 12, 13, 15, 17) or directly from the isotropic liquid (m = 18, 22). In planar cells no change of the extinction direction upon the transition from the nematic to smectic A phase was found, the optical axis remains along the rubbing direction and only a small increase of the birefringence was detected (Fig. 5), revealing that the smectic phase is orthogonal. In one-free-surface samples, a homeotropic texture was found, confirming the optical uniaxiality of the smectic A phase (Fig. 6). For dimers with m = 13–18, below the narrow temperature range of the SmA phase, two additional smectic phases were observed, the upper one (SmX) exhibiting a birefringent texture and the lower (SmC_{TB}) a homeotropic texture (Fig. 6) in one-surface-free samples. In a wedge cell with homeotropic anchoring, the upper

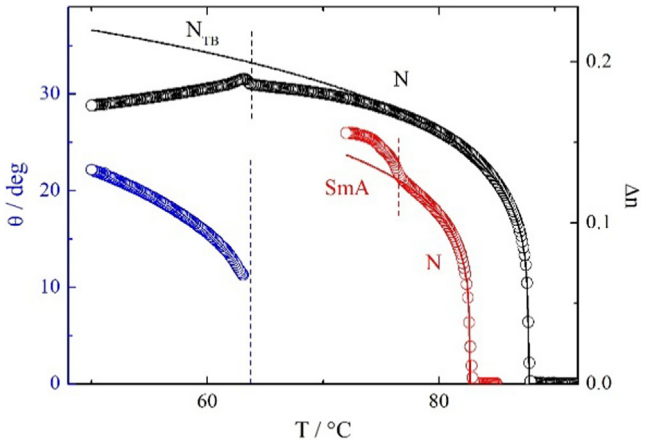

Fig. 5. Optical birefringence of CB6O.S9 (black circles) and CB6O.S17 (red circles). Lines show the power law temperature dependence $\Delta n = \Delta n_{max}\left(\frac{T_c - T}{T_c}\right)^{\beta}$, with Δn_{max} being 0.355 and 0.302 for CB6O.S9 and CB6O.S17, respectively, and critical exponent $\beta = 0.21$ for both compounds. The decrease in the measured birefringence in the N_{TB} phase of compound CB6O.S9 allowed for the determination of the heliconical tilt angle, θ (blue circles).

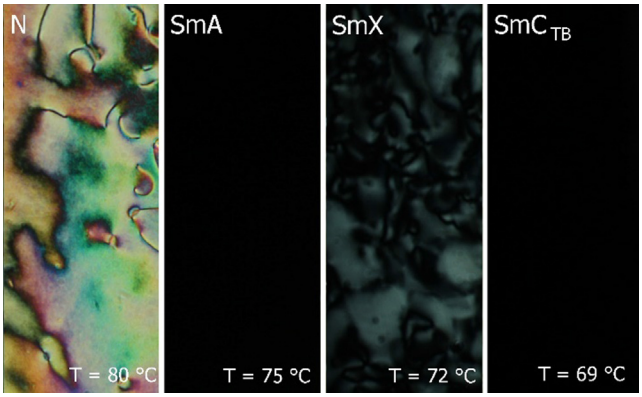

Fig. 6. Optical textures observed on cooling a one-free-surface sample of CB6O.S15.

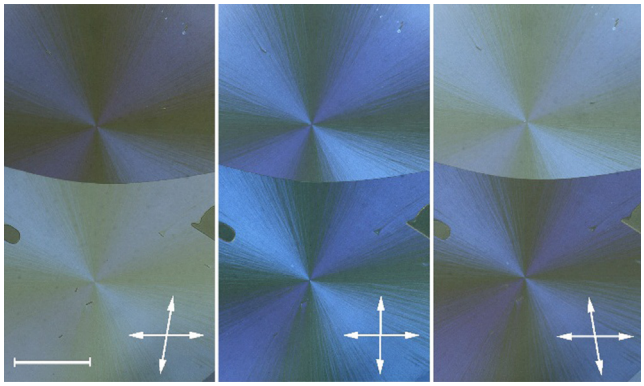

Fig. 7. Weakly birefringent, optically active domains of the B_4 phase of CB6O.S15, observed between crossed and slightly de-crossed (by 3 deg.) polarizers. Scale bar corresponds to 200 μm.

phase texture is decorated with dynamically moving stripes (Fig. 3d), such a texture was ascribed to the biaxial smectic A phase, SmA_b [39], an orthogonal smectic phase in which molecular rotation around the long axis is restricted. However, the birefringent texture of the SmX phase could also evidence a tilted SmC-like structure.

In a planar cell, careful observation of the SmX phase texture revealed the presence of lines on a uniform background (Fig. 3c), associated with regions of slightly higher birefringence. To determine whether SmX is an orthogonal SmA_b phase or tilted SmC phase we performed an experiment with doping the CB6O.S15 compound with small amount of chiral additive. As a result the SmX became optically uniaxial, giving perfect homeotropic texture. We concluded therefore that the SmX phase is tilted SmC-like phase, because the chiral doping promoted a helix formation and consequently the uniaxiality of the phase. The SmA_b phase would have been insensitive to chirality [40]. A similar phase sequence and associated textural changes were found for the CB6O.*m* series [41], suggesting that both tilted phases observed below SmA phase have heliconical structure (SmC_{TB}-type). However, the monotropic nature of all the smectic phases and rapid recrystallization precluded their detailed characterization.

Interestingly, when cooled rapidly in thin cells, all the dimers studied recrystallized into the B_4 phase ('blue crystal'), the characteristic feature of which is a twisted ribbon morphology [19]. It should be pointed out, however, that whereas for the longer homologues the B_4 crystal was stable at room temperature for months, the shorter homologues often displayed 'blue' crystals coexisting with other strongly birefringent crystalline phases and heating the sample resulted in a polymorphic transition from the metastable B_4 phase to the birefringent crystal. In calorimetric measurements B_4 phase was detected regardless of applied cooling rate (1–50 K min^{-1}), its formation was accompanied by enthalpy change of order of 50 kJ mol^{-1}. On heating, B_4 phase undergoes exothermic transition into another crystalline phase. The lamellar character of the B_4 phase was confirmed by X-ray diffraction studies (Fig. S1). The periodicity of the layered structure was found to be close to twice the molecular length, showing that the molecules are arranged in an antiparallel fashion in consecutive layers. The width of the diffraction signals was considerably broader than the instrumental resolution, and this is attributed to the limited width of the ribbons forming the helical filaments [20]. The B_4 phase showed a weakly birefringent (due to the not completely random orientation of the molecular layers), but an optically active texture (Fig. 7), and domains with opposite signs of the optical rotation were formed with equal probability. Given that these domains could be grown with dimensions comparable to the sample size, it was possible to prepare samples having a strong imbalance between opposite chirality domains enabling the measurement of circular dichroism (CD) spectra, see Fig. 8, and Figs S2 and S3 in the ESI. A strong CD signal was observed at the wavelength of the absorption edge of the compound in the solid state, ~400 nm (Fig. S2).

In order to correlate the optical rotatory power (ORP) and CD signal with the structure/morphology of the B_4 phase, the almost homochiral sample was further studied using AFM, which revealed membranes made of molecular layers with a number of strongly saddle-splay deformed areas randomly distributed in space (Fig. 9), resembling the morphology of the dark conglomerate phase [42]. No areas with clear helical filaments could be seen. The almost random distribution of the layer orientation is consistent with the low optical birefringence of the sample. The absence of a clear helical morphology also suggests that the chiral nature of the phase, which gives rise to optical activity, originates from the layer chirality [43] rather than from a helical morphology. To obtain more information about the phase morphology, the sample was aligned using porous anodic aluminium oxide (AAO) and imaged with SEM, and under such conditions helical twisted ribbons, with a helical pitch of ~120 nm, were observed (Fig. 9). Apparently, the morphology of the sample, *i.e.* filaments vs dark conglomerate phase, may be controlled, at least to some extent, by surface interactions, despite the crystalline nature of the phase. It has been recently reported [44] that limiting space for the nucleation of saddle-splay deformed layers promotes the formation of helical filaments growing along the AAO channel axis over

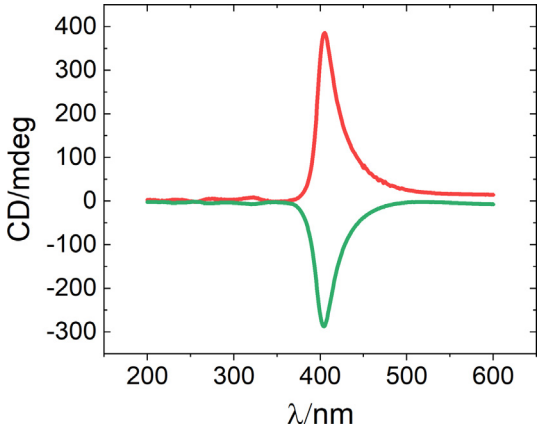

Fig. 8. CD spectra for two samples of CB6O.S18, with opposite chirality macroscopic domains of the B_4 crystal phase, thin films measured on quartz.

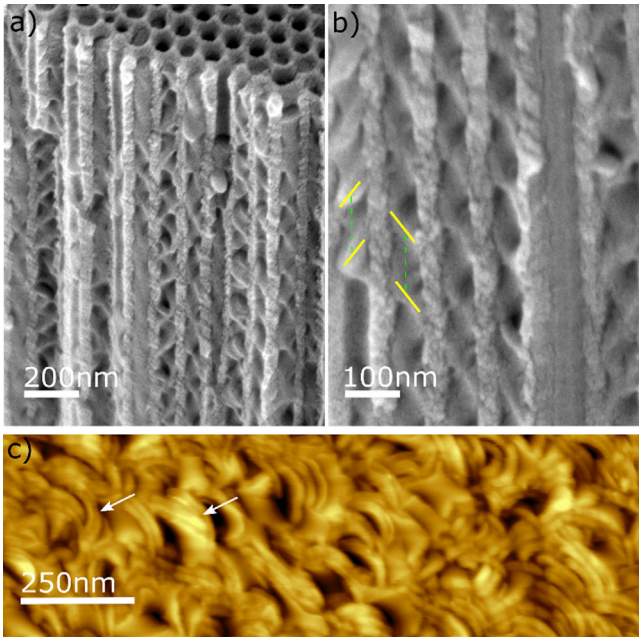

Fig. 9. (a, b) SEM images of helical filaments of B_4 phase of CB6O.S17 grown in an AAO template, each pore of the template has a 60 nm diameter, the pitch of both right- and left-handed filaments is approximately 120 nm. (c) AFM height image of the B_4 phase of CB6O.S18 on quartz, the randomly distributed strongly deformed membranes made of molecular layers (marked with arrows) are visible.

the formation of the 3-dimensional deformed dark conglomerate structures.

Comparing the thioalkyl CB6O.S*m* dimers studied here with the corresponding alkyloxy CB6O.O*m* [33] and alkyl CB6O.*m* series [32,41] reveals that the N-Iso transition temperatures, T_{NI}, are lowest for the mesogens having an alkylthio chain and highest for those with an alkyloxy chain. This may be attributed to the changes of bond angle between the mesogenic unit and the terminal chain, and the position of the chain with respect to the plane of the mesogenic unit. Thus, an alkyloxy chain lies more or less in the plane of the mesogenic core whereas the alkylthio and alkyl chains protrude at some angle. In addition, C-S-C is the smallest of the three bond angles and this reduces the overall molecular shape anisotropy. The exceptions to this behavior are CB6O.S1 and CB6O.S2, for which the isotropisation temperatures are considerably higher than expected. It has been suggested that this may be attributed to chalcogen bonding in these compounds [45]. Although such an interaction cannot be excluded in the liquid crystalline state, our X-ray diffraction studies show no direct S-S contact interactions in the crystalline state, while crystal packing appeared to maximize the amount of C-H...S interactions (Fig. S3-S6). Although the N-Iso transition temperatures of the CB6O.S*m* series tend to be lower, their melting points are higher than for the corresponding alkyl and alkyloxy series, resulting in the monotropic nature of the liquid crystalline phases that have a strong tendency to crystallize, this behavior can be attributed to presence of relatively strong C-H...S interactions (see SI). All three series, CB6O.S*m*, CB6O.O*m* and CB6O.*m*, show bilayer structures for long terminal chains, and intercalated structures for the shorter chains, with a gradual evolution of the molecular packing as the terminal chain length is changed. It should be stressed that for all three series, smectic phases were observed; for the CB6O.S*m* series for $m \geq 13$ and for CB6O.*m* series for $m \geq 10$. By comparison, the CB6O.O*m* series shows smectic behaviour only for intermediate length compounds, with m = 3, 4 and 5 [33]. The observation of smectic phase behavior for intermediate chain lengths only in the CB6O.O*m* series is thought to be related to the ability of these dimers to better pack into an intercalated structure, and this arises from both the alkyloxy chain lying in the plane of the benzylideneanline unit and the larger C-O-C bond angle compared to C-S-C.

4. Conclusions

We report the first series of flexible mesogenic dimers for which N_{TB} and B_4 phases are observed for a single compound as a function of temperature. Although the N_{TB} phase is relatively common in bent, flexible dimers, the formation of the B_4 phase for such molecules is unusual [20,46], this phase is normally observed for rigid bent core molecules [18,19,47]. The dimers reported here also form another type of helical phases, SmC_{TB}-type, which is the smectic analogue of the N_{TB} phase. Unfortunately, the monotropic nature of the smectic phases precluded their further investigation.

Funding

National Science Centre (Poland) under the grant no. 2016/22/A/ST5/00319.

Declaration of Competing Interest

The authors declare that they have no known competing financial interests or personal relationships that could have appeared to influence the work reported in this paper.

Acknowledgment

The work was financed by the National Science Centre (Poland) under the grant no. 2016/22/A/ST5/00319. Special acknowledgement and thanks to professor Dong Ki Yoon's group for providing the AAO membranes.

Appendix A. Supplementary data

Supplementary data to this article can be found online at https://doi.org/10.1016/j.molliq.2021.118180.

References

[1] T. Buhse, J.-M. Cruz, M.E. Noble-Terán, D. Hochberg, J.M. Ribó, J. Crusats, J.-C. Micheau, Spontaneous deracemizations, Chem. Rev. 121 (4) (2021) 2147–2229, https://doi.org/10.1021/acs.chemrev.0c00819.
[2] C. Tschierske, Mirror symmetry breaking in liquids and liquid crystals, Liq. Cryst. 45 (13-15) (2018) 2221–2252, https://doi.org/10.1080/02678292.2018.1501822.
[3] I. Dozov, On the spontaneous symmetry breaking in the mesophases of achiral banana-shaped molecules, Europhys. Lett. 56 (2) (2001) 247–253, https://doi.org/10.1209/epl/i2001-00513-x.
[4] V. Borshch, Y.K. Kim, J. Xiang, M. Gao, A. Jákli, V.P. Panov, J.K. Vij, C.T. Imrie, M. G. Tamba, G.H. Mehl, O.D. Lavrentovich, Nematic twist-bend phase with nanoscale modulation of molecular orientation, Nat. Commun. 4 (2013) 2635, https://doi.org/10.1038/ncomms3635.
[5] D. Chen, J.H. Porada, J.B. Hooper, A. Klittnick, Y. Shen, M.R. Tuchband, E. Korblova, D. Bedrov, D.M. Walba, M.A. Glaser, J.E. Maclennan, N.A. Clark, Chiral heliconical ground state of nanoscale pitch in a nematic liquid crystal of achiral molecular dimers, Proc. Natl. Acad. Sci. U. S. A. 110 (40) (2013) 15931–15936, https://doi.org/10.1073/pnas.1314654110.
[6] M. Cestari, S. Diez-Berart, D.A. Dunmur, A. Ferrarini, M.R. De La Fuente, D.J.B. Jackson, D.O. Lopez, G.R. Luckhurst, M.A. Perez-Jubindo, R.M. Richardson, J. Salud, B.A. Timimi, H. Zimmermann, Phase behavior and properties of the liquid-crystal dimer 1″,7″-bis(4-cyanobiphenyl-4′-yl) heptane: a twist-bend nematic liquid crystal, Phys. Rev. E - Stat. Nonlinear, Soft Matter Phys. 84 (2011) 31704, https://doi.org/10.1103/PhysRevE.84.031704.
[7] R. Walker, D. Pociecha, J.M.D. Storey, E. Gorecka, C.T. Imrie, The chiral twist-bend nematic phase (N*TB), Chem. – A Eur. J. 25 (58) (2019) 13329–13335, https://doi.org/10.1002/chem.201903014.
[8] R.J. Mandle, C.T. Archbold, J.P. Sarju, J.L. Andrews, J.W. Goodby, The dependency of nematic and twist-bend mesophase formation on bend angle, Sci. Rep. 6 (2016) 1–12, https://doi.org/10.1038/srep36682.
[9] E. Forsyth, D.A. Paterson, E. Cruickshank, G.J. Strachan, E. Gorecka, R. Walker, J. M.D. Storey, C.T. Imrie, Liquid crystal dimers and the twist-bend nematic

phase: on the role of spacers and terminal alkyl chains, J. Mol. Liq. 320 (2020) 114391, https://doi.org/10.1016/j.molliq.2020.114391.
[10] R. Walker, M. Majewska, D. Pociecha, A. Makal, J.M. Storey, E. Gorecka, C.T. Imrie, Twist-bend nematic glasses: the synthesis and characterisation of pyrene-based nonsymmetric dimers, ChemPhysChem. 22 (2021) 461–470, https://doi.org/10.1002/cphc.202000993.
[11] Y. Arakawa, K. Komatsu, S. Inui, H. Tsuji, Thioether-linked liquid crystal dimers and trimers: the twist-bend nematic phase, J. Mol. Struct. 1199 (2020) 126913, https://doi.org/10.1016/j.molstruc.2019.126913.
[12] D. Chen, M. Nakata, R. Shao, M.R. Tuchband, M. Shuai, U. Baumeister, W. Weissflog, D.M. Walba, M.A. Glaser, J.E. Maclennan, N.A. Clark, Twist-bend heliconical chiral nematic liquid crystal phase of an achiral rigid bent-core mesogen, Phys. Rev. E. 89 (2014) 22506, https://doi.org/10.1103/PhysRevE.89.022506.
[13] Y. Wang, G. Singh, D.M. Agra-Kooijman, M. Gao, H.K. Bisoyi, C. Xue, M.R. Fisch, S. Kumar, Q. Li, Room temperature heliconical twist-bend nematic liquid crystal, CrystEngComm. 17 (14) (2015) 2778–2782, https://doi.org/10.1039/C4CE02502D.
[14] S.P. Sreenilayam, Y.P. Panarin, J.K. Vij, V.P. Panov, A. Lehmann, M. Poppe, M. Prehm, C. Tschierske, Spontaneous helix formation in non-chiral bent-core liquid crystals with fast linear electro-optic effect, Nat. Commun. 71 (7) (2016) 1–8, https://doi.org/10.1038/ncomms11369.
[15] J.P. Abberley, R. Killah, R. Walker, J.M.D. Storey, C.T. Imrie, M. Salamończyk, C. Zhu, E. Gorecka, D. Pociecha, Heliconical smectic phases formed by achiral molecules, Nat. Commun. 9 (2018) 228, https://doi.org/10.1038/s41467-017-02626-6.
[16] M. Salamończyk, N. Vaupotič, D. Pociecha, R. Walker, J.M.D. Storey, C.T. Imrie, C. Wang, C. Zhu, E. Gorecka, Multi-level chirality in liquid crystals formed by achiral molecules, Nat. Commun. 10 (2019) 1922, https://doi.org/10.1038/s41467-019-09862-y.
[17] J.K. Vij, Y.P. Panarin, S.P. Sreenilayam, M. Alaasar, C. Tschierske, Investigation of the heliconical smectic <math xmlns, Phys. Rev. Mater. 3 (2019) 045603, https://doi.org/10.1103/PhysRevMaterials.3.045603.
[18] T. Sekine, T. Niori, J. Watanabe, T. Furukawa, S.W. Choi, H. Takezoe, Spontaneous helix formation in smectic liquid crystals comprisingachiral molecules, J. Mater. Chem. 7 (1997) 1307–1309, https://doi.org/10.1039/A702026K.
[19] L.E. Hough, H.T. Jung, D. Krüerke, M.S. Heberling, M. Nakata, C.D. Jones, D. Chen, D.R. Link, J. Zasadzinski, G. Heppke, J.P. Rabe, W. Stocker, E. Körblova, D. M. Walba, M.A. Glaser, N.A. Clark, Helical nanofilament phases, Science. 325 (5939) (2009) 456–460.
[20] E. Białecka-Florjańczyk, I. Śledzińska, E. Górecka, J. Przedmojski, Odd–even effect in biphenyl-based symmetrical dimers with methylene spacer – evidence of the B4 phase, Liq. Cryst. 35 (4) (2008) 401–406, https://doi.org/10.1080/02678290801906052.
[21] D.A. Paterson, M. Gao, Y.K. Kim, A. Jamali, K.L. Finley, B. Robles-Hernández, S. Diez-Berart, J. Salud, M.R. De La Fuente, B.A. Timimi, H. Zimmermann, C. Greco, A. Ferrarini, J.M.D. Storey, D.O. López, O.D. Lavrentovich, G.R. Luckhurst, C.T. Imrie, Understanding the twist-bend nematic phase: the characterisation of 1-(4-cyanobiphenyl-4′-yloxy)-6-(4-cyanobiphenyl-4′-yl)hexane (CB6OCB) and comparison with CB7CB, Soft Matter. 12 (2016) 6827–6840, https://doi.org/10.1039/c6sm00537c.
[22] D.A. Paterson, R. Walker, J.P. Abberley, J. Forestier, W.T.A. Harrison, J.M.D. Storey, D. Pociecha, E. Gorecka, C.T. Imrie, Azobenzene-based liquid crystal dimers and the twist-bend nematic phase, Liq. Cryst. 44 (2017) 2060–2078, https://doi.org/10.1080/02678292.2017.1366075.
[23] Y. Arakawa, S. Inui, K. Igawa, H. Tsuji, Alkylthio- and alkyl-substituted asymmetric diphenyldiacetylene-based liquid crystals: phase transitions, mesophase and single-crystal structures, and birefringence, Liq. Cryst. 46 (2019) 1621–1630, https://doi.org/10.1080/02678292.2019.1590744.
[24] Y. Arakawa, Y. Sasaki, N. Haraguchi, S. Itsuno, H. Tsuji, Synthesis, phase transitions and birefringence of novel liquid crystalline 1,4-phenylene bis(4-alkylthio benzoates) and insights into the cybotactic nematic behaviour, Liq. Cryst. 45 (6) (2018) 821–830, https://doi.org/10.1080/02678292.2017.1385103.
[25] Y. Arakawa, S. Kang, H. Tsuji, J. Watanabe, G.-I. Konishi, Development of novel bistolane-based liquid crystalline molecules with an alkylsulfanyl group for highly birefringent materials, RSC Adv. 6 (20) (2016) 16568–16574.
[26] J. Xiang, A. Varanytsia, F. Minkowski, D.A. Paterson, J.M.D. Storey, C.T. Imrie, O.D. Lavrentovich, P. Palffy-Muhoray, Electrically tunable laser based on oblique heliconical cholesteric liquid crystal, Proc. Natl. Acad. Sci. U. S. A. 113 (46) (2016) 12925–12928, https://doi.org/10.1073/pnas.1612212113.
[27] J. Xiang, Y. Li, Q. Li, D.A. Paterson, J.M.D. Storey, C.T. Imrie, O.D. Lavrentovich, Electrically tunable selective reflection of light from ultraviolet to visible and infrared by heliconical cholesterics, Adv. Mater. 27 (19) (2015) 3014–3018, https://doi.org/10.1002/adma.201500340.
[28] Y. Arakawa, Y. Ishida, H. Tsuji, Ether- and thioether-linked naphthalene-based liquid-crystal dimers: influence of chalcogen linkage and mesogenic-arm symmetry on the incidence and stability of the twist-bend nematic phase, Chem. – A Eur. J. 26 (2020) 3767–3775, https://doi.org/10.1002/chem.201905208.
[29] Y. Arakawa, K. Komatsu, H. Tsuji, Twist-bend nematic liquid crystals based on thioether linkage, New J. Chem. 43 (17) (2019) 6786–6793.
[30] E. Cruickshank, M. Salamończyk, D. Pociecha, G.J. Strachan, J.M.D. Storey, C. Wang, J. Feng, C. Zhu, E. Gorecka, C.T. Imrie, Sulfur-linked cyanobiphenyl-based liquid crystal dimers and the twist-bend nematic phase, Liq. Cryst. 46 (10) (2019) 1595–1609, https://doi.org/10.1080/02678292.2019.1641638.
[31] H.-C. Lee, Z. Lu, P.A. Henderson, M.F. Achard, W.A.K. Mahmood, G.-Y. Yeap, C.T. Imrie, Cholesteryl-based liquid crystal dimers containing a sulfur–sulfur link in the flexible spacer, Liq. Cryst. 39 (2) (2012) 259–268, https://doi.org/10.1080/02678292.2011.641753.
[32] R. Walker, D. Pociecha, G.J. Strachan, J.M.D. Storey, E. Gorecka, C.T. Imrie, Molecular curvature, specific intermolecular interactions and the twist-bend nematic phase: the synthesis and characterisation of the 1-(4-cyanobiphenyl-4′-yl)-6-(4-alkylanilinebenzylidene-4′-oxy)hexanes (CB6O.m), Soft Matter. 15 (2019) 3188–3197, https://doi.org/10.1039/c9sm00026g.
[33] D.A. Paterson, C.A. Crawford, D. Pociecha, R. Walker, J.M.D. Storey, E. Gorecka, C.T. Imrie, The role of a terminal chain in promoting the twist-bend nematic phase: the synthesis and characterisation of the 1-(4-cyanobiphenyl-4′-yl)-6-(4-alkyloxyanilinebenzylidene-4′-oxy)hexanes, Liq. Cryst. 45 (2018) 2341–2351, https://doi.org/10.1080/02678292.2018.1525503.
[34] N. Avci, V. Borshch, D.D. Sarkar, R. Deb, G. Venkatesh, T. Turiv, S.V. Shiyanovskii, N.V.S. Rao, O.D. Lavrentovich, Viscoelasticity, dielectric anisotropy, and birefringence in the nematic phase of three four-ring bent-core liquid crystals with an L-shaped molecular frame, Soft Matter. 9 (4) (2013) 1066–1075.
[35] S. Lee, H. Kim, E. Tsai, J.M. Richardson, E. Korblova, D.M. Walba, N.A. Clark, S.B. Lee, D.K. Yoon, Multidimensional helical nanostructures in multiscale nanochannels, Langmuir. 31 (29) (2015) 8156–8161, https://doi.org/10.1021/acs.langmuir.5b01620.
[36] M. Ali, E. Gorecka, D. Pociecha, N. Vaupotič, Structure and grating efficiency of thin cells filled by a twist-bend nematic liquid crystal, Phys. Rev. E. 102 (2020) 032704, https://doi.org/10.1103/PhysRevE.102.032704.
[37] C. Meyer, G.R. Luckhurst, I. Dozov, The temperature dependence of the heliconical tilt angle in the twist-bend nematic phase of the odd dimer CB7CB, J. Mater. Chem. C. 3 (2) (2015) 318–328.
[38] D. Pociecha, C. Crawford, D.A. Paterson, J.M.D. Storey, C.T. Imrie, N. Vaupotič, E. Gorecka, Nature of nematic to twist bend nematic phase transition, Phys. Rev. E. 98 (2018) 052706, https://doi.org/10.1103/PhysRevE.98.052706.
[39] B.K. Sadashiva, R. Amaranatha Reddy, R. Pratibha, N.V. Madhusudana, Biaxial smectic A phase in homologous series of compounds composed of highly polar unsymmetrically substituted bent-core molecules, J. Mater. Chem. 12 (2002) 943–950, https://doi.org/10.1039/b109546c.
[40] V. Padmini, P.N. Babu, G.G. Nair, D.S.S. Rao, C.V. Yelamaggad, Optically biaxial, re-entrant and frustrated mesophases in chiral, non-symmetric liquid crystal dimers and binary mixtures, Chem. – Asian J. 11 (20) (2016) 2897–2910, https://doi.org/10.1002/asia.201600918.
[41] D. Pociecha, N. Vaupotič, M. Majewska, E. Cruickshank, R. Walker, J.M.D. Storey, C.T. Imrie, C. Wang, E. Gorecka, Photonic bandgap in achiral liquid crystals—a twist on a twist, Adv. Mater. (2021) 2103288, https://doi.org/10.1002/ADMA.202103288.
[42] L.E. Hough, M. Spannuth, M. Nakata, D.A. Coleman, C.D. Jones, G. Dantlgraber, C. Tschierske, J. Watanabe, E. Körblova, D.M. Walba, J.E. Maclennan, M.A. Glaser, N.A. Clark, Chiral isotropic liquids from achiral molecules, Science. 325 (5939) (2009) 452–456.
[43] J. Matraszek, N. Topnani, N. Vaupotič, H. Takezoe, J. Mieczkowski, D. Pociecha, E. Gorecka, Monolayer filaments versus multilayer stacking of bent-core molecules, Angew. Chemie Int. Ed. 55 (10) (2016) 3468–3472, https://doi.org/10.1002/anie.201510123.
[44] L. Foley, W. Park, M. Yang, E. Carlson, E. Korblova, D.K. Yoon, D.M. Walba, Nanoconfinement of the low-temperature dark conglomerate: structural control from focal conics to helical nanofilaments, Chem. – A Eur. J. 25 (2019) 7438–7442, https://doi.org/10.1002/CHEM.201900653.
[45] E. Cruickshank, G.J. Strachan, J.M. Storey, C.T. Imrie, Chalcogen bonding and liquid crystallinity: Understanding the anomalous behaviour of the 4′-(alkylthio)[1,1′-biphenyl]-4-carbonitriles (nSCB), J. Mol. Liq. (2021) 117094, https://doi.org/10.1016/J.MOLLIQ.2021.117094.
[46] A. Zep, K. Sitkowska, D. Pociecha, E. Gorecka, Photoresponsive helical nanofilaments of B4 phase, J. Mater. Chem. C. 2 (13) (2014) 2323–2327.
[47] E. Tsai, J.M. Richardson, E. Korblova, M. Nakata, D. Chen, Y. Shen, R. Shao, N.A. Clark, D.M. Walba, A modulated helical nanofilament phase, Angew. Chemie. 52 (20) (2013) 5254–5257.

Supplementary Information

Helical phases assembled from achiral molecules: twist-bend nematic and helical filamentary B_4 phases formed by mesogenic dimers

E. Cruickshank,[1] K. Anderson,[2] J. M. D. Storey,[1] C.T. Imrie,[1] E. Gorecka,[2] D. Pociecha,[2] M. M. Majewska[2]*

[1] *Department of Chemistry, School of Natural and Computing Sciences, University of Aberdeen, Meston Building, Aberdeen AB24 3UE (UK)*

[2] *Faculty of Chemistry, University of Warsaw, ul. Zwirki i Wigury 101, 02-089 Warsaw (Poland)*

**Author for correspondence, E-mail: mmajewska@chem.uw.edu.pl*

Contents

S 1. Synthesis

S 1.1 Materials and Methods

Reagents All reagents and solvents that were available commercially were purchased from Sigma Aldrich, Fisher Scientific, TCI Chemicals or Fluorochem and were used without further purification unless otherwise stated.

Thin Layer Chromatography Reactions were monitored using thin layer chromatography and the appropriate solvent system using aluminium-backed plates with a coating of Merck Kieselgel 60 F254 silica which were purchased from Merck KGaA. The spots on the plate were visualised by UV light (254 nm) or by oxidation using either a potassium permanganate stain or iodine dip.

Column Chromatography For normal phase column chromatography, the separations were carried out using silica gel grade 60 Å, 40-63 μm particle size, purchased from Fluorochem and using an appropriate solvent system. In addition, some normal phase separations were carried out using a Biotage Selekt system with Biotage Sfar Silica High Capacity Duo Columns of 50 g or 100 g load capacity. The desired spots were identified using a UV detector which was set to 254 nm and the instrument collected the spots when a threshold of 250 mAU was surpassed.

Structure Characterization All final products and intermediates that were synthesised were characterised using ^{1}H NMR, ^{13}C NMR and infrared spectroscopies. The ^{1}H and ^{13}C NMR spectra were recorded on either a 400 MHz Bruker Avance III HD NMR spectrometer, or a 300 MHz Bruker Ultrashield NMR spectrometer. The infrared spectra were recorded on a Thermal Scientific Nicolet IR100 FTIR spectrometer with an ATR diamond cell.

Purity Analysis In order to determine the purity of the final products, elemental analysis was used. C, H, N, S microanalysis were carried out by the Sheffield Analytical and Scientific Services Elemental Microanalysis Service at the University of Sheffield using an Elementar Vario MICRO Cube or by the Elemental Analysis Service at OEA Laboratories Limited using a CE Instruments EA1110 CHNS-O Elemental Analyser. The instruments were calibrated using series of different masses of sulphanilamide and acetanilide.

S 1.2 Synthesis of the CB6O.Sm series

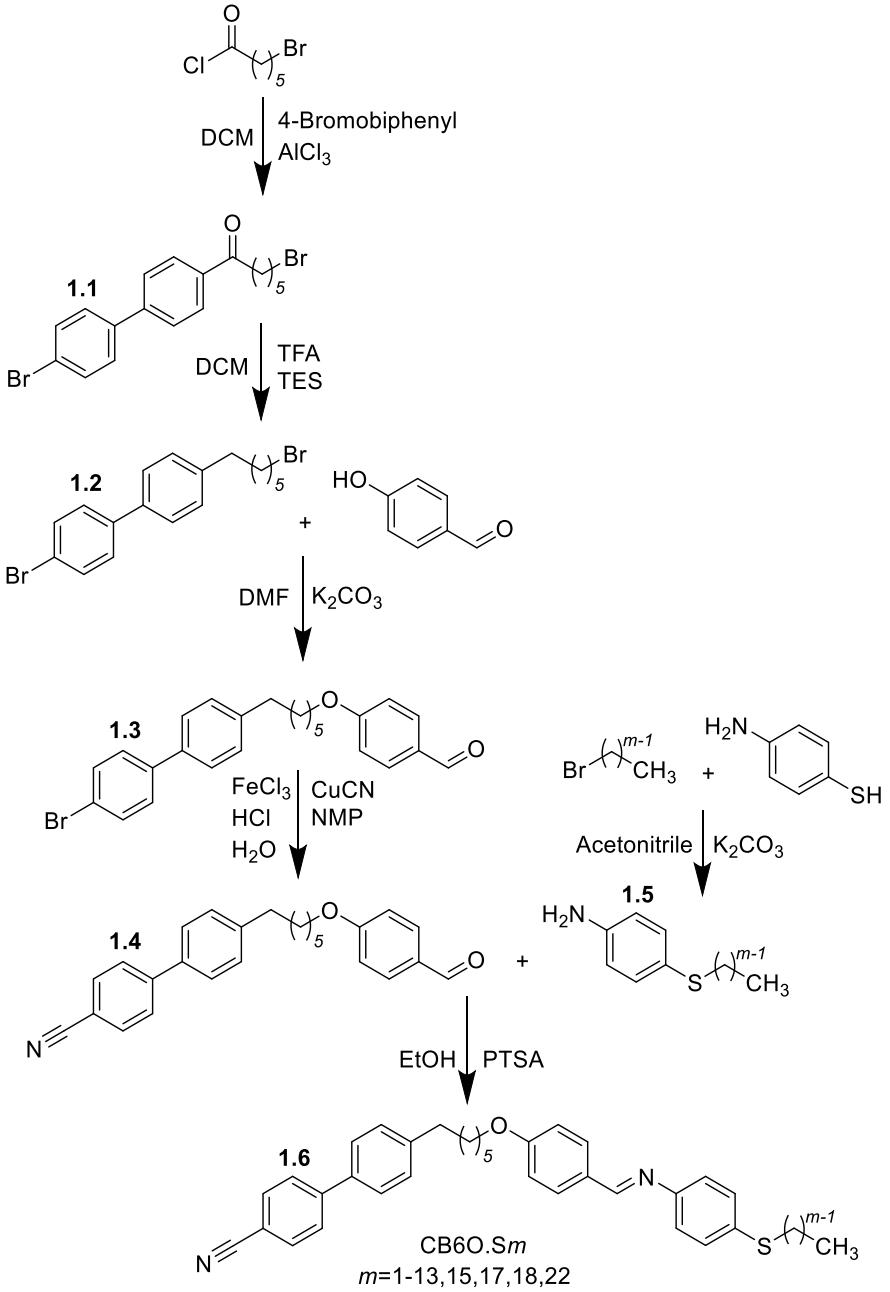

Scheme S 1. Synthesis of CB6O.S*m*.

The synthesis of the CB6O.S*m* series follows the steps outlined in **Scheme S1**. In the synthesis of the CB6O.S*m* series, the bromoalkanoyl chloride underwent a Friedel-Crafts acylation, hydrosilane reduction, Williamson's ether reaction and a Rosenmund-von Braun cyanation reaction in a method described by Abberley *et al*[1] to form the aldehyde intermediate (**1.4**). A modified Williamson's ether reaction[2] was used to synthesise the aniline intermediate (**1.5**). The aldehyde and aniline intermediates were subsequently combined in a Schiff's base reaction[3] to form the desired product.

S 1.2.1 6-Bromo-1-(4'-bromo[1,1'-biphenyl]-4-yl)hexan-1-one (1.1)

To pre-dried flask flushed with argon, aluminium chloride (7.25 g, 0.0564 mol) was added along with dry dichloromethane (60 mL) while being stirred. The outside of the flask was wrapped in tinfoil to prevent light from interfering with the reaction and was placed into an ice bath in order to keep the reaction mixture at 0 °C. 4-Bromobiphenyl (12.1 g, 0.0517 mol) and 6-bromohexanoyl chloride (7.19 mL, 10.0 g, 0.0470 mol) were mixed along with dry dichloromethane (60 mL) before being added dropwise into the flask. The ice bath was removed, and the reaction proceeded at room temperature overnight. The reaction was monitored by TLC using 100 % dichloromethane as the solvent system (RF value quoted in the product data). The mixture was then added to a slurry of ice (50 g) with 6 M hydrochloric acid (12 mL) and extracted with dichloromethane (200 mL). The extracted organic layer was washed with water (3 × 50 mL) and dried over anhydrous magnesium sulfate. The magnesium sulfate was removed using vacuum filtration and the filtrate collected, followed by the solvent being evaporated under vacuum to leave an off-white solid which was recrystalised using hot ethanol (250 mL).

Yield: 10.15 g, 53.2 %. RF: 0.53. MP: 81 °C

ν_{max}/cm^{-1}: 2938, 1678, 1604, 1477, 1389, 1365, 1262, 1208, 1189, 1070, 1000, 969, 822, 794, 723, 664, 574

δ_H/ppm (400 MHz, $CDCl_3$): 8.02 (2 H, d, J 8.3 Hz, Ar-H), 7.65 (2 H, d, J 8.3 Hz, Ar-H), 7.59 (2 H, d, J 8.4 Hz, Ar-H), 7.49 (2 H, d, J 8.4 Hz, Ar-H), 3.44 (2 H, t, J 7.1 Hz, Br-$\underline{CH_2}$-CH_2-), 3.03 (2 H, t, J 7.1 Hz, C(=O)-$\underline{CH_2}$-CH_2-), 1.93 (2 H, quin, J 7.1 Hz, Br-CH_2-$\underline{CH_2}$-CH_2-), 1.79 (2 H, quin, J 7.1 Hz, C(=O)-CH_2-$\underline{CH_2}$-CH_2-), 1.56 (2 H, quin, J 7.1 Hz, Br-CH_2-CH_2-$\underline{CH_2}$-CH_2-)

δ_C/ppm (100 MHz, $CDCl_3$): 199.45, 144.40, 138.78, 135.94, 132.11, 128.82, 128.73, 127.07, 122.66, 38.37, 33.65, 32.64, 27.90, 23.37

Data consistent with reported values [1]

S 1.2.2 4-Bromo-4'-(6-bromohexyl)-1,1'-biphenyl (1.2)

To a pre-dried flask flushed with argon, compound **1.1** (10.0 g, 0.0244 mol) was added. The flask was then placed into an ice bath in order to maintain the temperature at 0 °C. The solid was solubilised using trifluoroacetic acid (100 mL, 149 g, 1.31 mol) and dry dichloromethane (40 mL) along with stirring. Finally, triethylsilane (20.0 mL, 14.6 g, 0.125 mol) was added to

the flask and the ice bath was removed. The reaction was left for 24 hours and monitored by TLC using 100 % dichloromethane as the solvent system (RF values quoted in the product data). Once complete, the mixture was added to a beaker with dichloromethane (100 mL) and water (300 mL). The organic layer was separated and washed with water (3 × 50 mL). This was then dried using anhydrous magnesium sulfate, which was removed by vacuum filtration and the filtrate collected. The solvent was evaporated under vacuum to leave a white solid which was recrystalised using hot ethanol (150 mL).

Yield: 6.77 g, 70.8 %. RF: 0.67. MP: 76 °C

ν_{max}/cm^{-1}: 2931, 2856, 1479, 1454, 1390, 1235, 1189, 1077, 1000, 804, 726, 646, 503

δ_H/ppm (400 MHz, $CDCl_3$): 7.55 (2 H, d, J 8.2 Hz, Ar-H), 7.46 (4 H, t, J 8.2 Hz, Ar-H), 7.24 (2 H, d, J 8.2 Hz, Ar-H), 3.41 (2 H, t, J 6.8 Hz, Br-$\underline{CH_2}$-CH_2-), 2.66 (2 H, t, J 7.3 Hz, Ar-$\underline{CH_2}$-CH_2-), 1.87 (2 H, tt, J 7.3 Hz, 6.8 Hz, Br-CH_2-$\underline{CH_2}$-CH_2-), 1.67 (2 H, quin, J 7.3 Hz, Ar-CH_2-$\underline{CH_2}$-CH_2-), 1.48 (2 H, quin, J 7.3 Hz, Br-CH_2-CH_2-$\underline{CH_2}$-CH_2-), 1.40 (2 H, quin, J 7.3 Hz, Ar-CH_2-CH_2-$\underline{CH_2}$-CH_2-)

δ_C/ppm (100 MHz, $CDCl_3$) 142.18, 140.03, 137.42, 131.81, 128.96, 128.57, 126.82, 121.21, 35.44, 33.95, 32.73, 31.21, 28.40, 28.03

Data consistent with reported values [1]

S 1.2.3 4-{[6-(4'-Bromo[1,1'-biphenyl]-4-yl)hexyl]oxy}benzaldehyde (1.3)

To a pre-dried flask flushed with argon and fitted with a condenser, 4-hydroxybenzaldehyde (1.87 g, 0.0153 mol) and potassium carbonate (3.84 g, 0.0278 mol) were added. Dimethylformamide (30 mL) was added with compound **1.2** (5.51 g, 0.0139 mol) and then stirred. The reaction was heated to 90 °C and left overnight and monitored by TLC using 100 % dichloromethane as the solvent system (RF value quoted in the product data). The reaction mixture was then cooled to room temperature, before being poured into water (150 mL). The resulting white precipitate was vacuum filtered, and the collected white powder was recrystallised from hot ethanol (100 mL).

Yield: 3.64 g, 60.0 %. RF: 0.33. MP: 92 °C

ν_{max}/cm^{-1}: 2930, 2857, 1691, 1600, 1577, 1507, 1481, 1431, 1392, 1300, 1243, 1216, 1166, 1106, 1078, 1012, 1001, 837, 805, 767, 752, 732, 652, 619, 517, 505, 481

δ_H/ppm (400 MHz, $CDCl_3$): 9.88 (1 H, s, (C=O)-H), 7.82 (2 H, d, J 8.3 Hz, Ar-H), 7.55 (2 H, d, J 8.0 Hz, Ar-H), 7.46 (4 H, m, Ar-H), 7.25 (2 H, d, J 7.7 Hz, Ar-H), 6.98 (2 H, d, J 8.3 Hz, Ar-H), 4.04 (2 H, t, J 6.5 Hz, O-$\underline{CH_2}$-CH_2-), 2.67 (2 H, t, J 7.6 Hz, Ar-$\underline{CH_2}$-CH_2-), 1.83 (2 H,

tt, J 6.9 Hz, 6.5 Hz, O-CH_2-$\underline{CH_2}$-CH_2-), 1.71 (2 H, quin, J 7.6 Hz, Ar-CH_2-$\underline{CH_2}$-CH_2-), 1.45 (4 H, m, Ar-CH_2-CH_2-$\underline{CH_2}$-$\underline{CH_2}$-CH_2-)

δ_C/ppm (100 MHz, $CDCl_3$): 190.80, 164.21, 142.22, 140.00, 137.41, 132.00, 131.82, 129.79, 128.97, 128.55, 126.81, 121.22, 114.75, 68.32, 35.47, 31.30, 28.99, 28.94, 25.87

Data consistent with reported values [1]

SI1.2.4 4'-[6-(4-Formylphenoxy)hexyl][1,1'-biphenyl]-4-carbonitrile (1.4)

To a pre-dried flask flushed with argon and fitted with a condenser, compound **1.3** (5.25 g, 0.0120 mol) was added along with n-methyl-2-pyrrilidone (50 mL) and then stirred. In addition, the flask was connected to a Drechsel bottle filled with sodium hypochlorite. Using respiration protection, copper (I) cyanide (2.15 g, 0.0240 mol) was added to the flask and all equipment used placed into a sodium hypochlorite bath for 24 hours. The mixture was then heated to 200 °C for 4 hours to allow the reaction to proceed. In a separate flask, iron (III) chloride (19.5 g, 0.120 mol), 32 % hydrochloric acid (18.8 mL, 21.9 g, 0.600 mol) and water (45 mL) were all added together and mixed at 60 °C. The cyanide mixture was then cooled to 60 °C and once it reached this temperature the iron mixture was added to it. The resultant mixture was kept at 60 °C for 30 minutes before then being cooled to room temperature. The mixture was then stirred at room temperature for an hour before being added to a beaker containing water (200 mL) and dichloromethane (200 mL). The organic layer was separated and washed with water (3 × 100 mL). The organic layer was then dried using anhydrous magnesium sulfate. The magnesium sulfate was removed using vacuum filtration and the filtrate collected. The solvent was evaporated under vacuum to leave a brown liquid. This liquid was added to water (200 mL) which generated a brown precipitate which was collected by vacuum filtration. The crude product was purified using a silica gel column with 10 % 40:60 petroleum ether and 90 % dichloromethane as eluent (RF value quoted in product data). The eluent fractions of interest were evaporated under vacuum to leave an off-white/pale yellow solid which was recrystallised from hot ethanol (40 mL).

Yield: 2.82 g, 61.3 %. RF: 0.16

T_{Cr-}: 84 °C T_{NI} (46 °C)

ν_{max}/cm^{-1}: 2943, 2852, 2221, 1689, 1598, 1574, 1508, 1492, 1472, 1422, 1396, 1313, 1302, 1249, 1211, 1160, 1111, 1031, 1005, 846, 834, 813, 781, 647, 620, 546, 516

δ_H/ppm (400 MHz, $CDCl_3$): 9.88 (1 H, s, (C=O)-H), 7.82 (2 H, d, J 8.3 Hz, Ar-H), 7.71 (2 H, d, J 8.0 Hz, Ar-H), 7.66 (2 H, d, J 8.0 Hz, Ar-H), 7.51 (2 H, d, J 7.8 Hz, Ar-H), 7.28 (2 H, d, J 7.8 Hz, Ar-H), 6.98 (2 H, d, J 8.3 Hz, Ar-H), 4.04 (2 H, t, J 6.5 Hz, O-$\underline{CH_2}$-CH_2-), 2.69 (2 H,

t, J 7.7 Hz, Ar-$\underline{CH_2}$-CH_2-), 1.83 (2 H, tt, J 7.1 Hz, 6.5 Hz, O-CH_2-$\underline{CH_2}$-CH_2-), 1.70 (2 H, quin, J 7.7 Hz, Ar-CH_2-$\underline{CH_2}$-CH_2-), 1.48 (4 H, m, Ar-CH_2-CH_2-$\underline{CH_2}$-$\underline{CH_2}$-CH_2-)

δ_C/ppm (100 MHz, $CDCl_3$): 190.78, 164.18, 145.54, 143.44, 136.58, 132.58, 131.99, 129.81, 129.18, 127.48, 127.12, 119.02, 114.74, 110.60, 68.29, 35.51, 31.25, 28.99, 28.94, 25.86

Data consistent with reported values [1]

SI1.2.5 4-(Alkylthio)anilines (1.5)

To a pre-dried flask flushed with argon and fitted with a condenser, 4-aminothiophenol (1 eq) and potassium carbonate (2 eq) were added. Acetonitrile (50 mL) was added with the appropriate 1-bromoalkane (1.1 eq) and then stirred. The quantities of reagents used in each reaction are listed in **Table SI1.1**. The reaction was refluxed overnight and monitored by TLC using 100 % dichloromethane as the solvent system (RF values quoted in the product data). The reaction mixture was then vacuum filtered and then the solvent was removed under vacuum to give a brown oil. The crude product was purified using a 50 g Biotage column (program: 25 % dichloromethane and 75 % 40:60 petroleum ether for 1.5 column volumes, 30 % dichloromethane and 70 % 40:60 petroleum ether for 2 column volumes, 37 % dichloromethane and 63 % 40:60 petroleum ether for 3.5 column volumes, 97 % dichloromethane and 3 % 40:60 petroleum ether for 3 column volumes). The eluent fractions of interest were evaporated under vacuum give a brown oil or solid. The collected brown solids were recrystallised from hot ethanol (50 mL).

4-(Methylthio)aniline - Was purchased commercially from Sigma Aldrich and used without further purification.

4-(Ethylthio)aniline

Brown oil. Yield: 1.40 g, 38.1 %. RF: 0.30

ν_{max}/cm^{-1}: 3461, 3550, 3211, 2971, 2923, 1618, 1594, 1493, 1448, 1277, 1257, 1176, 819, 763, 621, 511

δ_H/ppm (400 MHz, $CDCl_3$): 7.24 (2 H, d, J 8.5 Hz, Ar-H), 6.62 (2 H, d, J 8.5 Hz, Ar-H), 3.69 (2H, br, NH_2), 2.79 (2 H, quart, J 7.4 Hz, S-$\underline{CH_2}$-CH_3), 1.23 (3 H, t, J 7.4 Hz, S-CH_2-$\underline{CH_3}$)

δ_C/ppm (100 MHz, $CDCl_3$): 145.85, 133.95, 123.34, 115.55, 30.37, 14.72

Data consistent with reported values [4]

Table S 1.1 Quantities of 1-bromoalkane used in the syntheses of 4-(alkylthio)anilines (**1.5**).

m	1-Bromoalkane	4-Aminothiophenol	Potassium carbonate
2	1.97 mL, 2.88 g, 0.0264 mol	3.00 g, 0.024 mol	6.63 g, 0.048 mol
3	2.40 mL, 3.25 g, 0.0264 mol	3.00 g, 0.024 mol	6.63 g, 0.048 mol
4	2.83 mL, 3.62 g, 0.0264 mol	3.00 g, 0.024 mol	6.63 g, 0.048 mol
5	3.27 mL, 3.99 g, 0.0264 mol	3.00 g, 0.024 mol	6.63 g, 0.048 mol
6	3.71 mL, 4.36 g, 0.0264 mol	3.00 g, 0.024 mol	6.63 g, 0.048 mol
7	4.15 mL, 4.73 g, 0.0264 mol	3.00 g, 0.024 mol	6.63 g, 0.048 mol
8	4.56 mL, 5.10 g, 0.0264 mol	3.00 g, 0.024 mol	6.63 g, 0.048 mol
9	5.04 mL, 5.47 g, 0.0264 mol	3.00 g, 0.024 mol	6.63 g, 0.048 mol
10	1.83 mL, 1.95 g, 8.80×10^{-3} mol	1.00 g, 8.00×10^{-3} mol	2.21 g, 0.0160 mol
11	1.97 mL, 2.07 g, 8.80×10^{-3} mol	1.00 g, 8.00×10^{-3} mol	2.21 g, 0.0160 mol
12	2.11 mL, 2.19 g, 8.80×10^{-3} mol	1.00 g, 8.00×10^{-3} mol	2.21 g, 0.0160 mol
13	2.25 mL, 2.32 g, 8.80×10^{-3} mol	1.00 g, 8.00×10^{-3} mol	2.21 g, 0.0160 mol
15	2.55 mL, 2.56 g, 8.80×10^{-3} mol	1.00 g, 8.00×10^{-3} mol	2.21 g, 0.0160 mol
17	2.81 g, 8.80×10^{-3} mol	1.00 g, 8.00×10^{-3} mol	2.21 g, 0.0160 mol
18	2.99 g, 8.80×10^{-3} mol	1.00 g, 8.00×10^{-3} mol	2.21 g, 0.0160 mol
22	3.43 g, 8.80×10^{-3} mol	1.00 g, 8.00×10^{-3} mol	2.21 g, 0.0160 mol

4-(Propylthio)aniline

Brown oil. Yield: 1.19 g, 29.6 %. RF: 0.34

ν_{max}/cm^{-1}: 3462, 3352, 3210, 2959, 2870, 1618, 1596, 1493, 1459, 1278, 1235, 1176, 819, 672, 623, 511

δ_H/ppm (400 MHz, $CDCl_3$): 7.23 (2 H, d, J 8.0 Hz, Ar-H), 6.61 (2 H, d, J 8.0 Hz, Ar-H), 3.65 (2 H, br, NH_2), 2.74 (2 H, t, J 7.3 Hz, S-$\underline{CH_2}$-CH_2-), 1.58 (2 H, sext, J 7.3 Hz, S-CH_2-$\underline{CH_2}$-CH_3), 0.97 (3 H, t, J 7.3 Hz, S-CH_2-CH_2-$\underline{CH_3}$)

δ_C/ppm (100 MHz, $CDCl_3$): 145.59, 133.78, 123.83, 115.54, 38.42, 22.71, 13.31

Data consistent with reported values [5]

4-(Butylthio)aniline

Brown oil. Yield: 0.740 g, 17.0 %. RF: 0.35

ν_{max}/cm^{-1}: 3462, 3354, 3211, 2955, 2927, 2870, 1618, 1596, 1493, 1463, 1273, 1175, 819, 727, 623, 513

δ_H/ppm (400 MHz, $CDCl_3$): 7.23 (2 H, d, J 8.4 Hz, Ar-H), 6.61 (2 H, d, J 8.4 Hz, Ar-H), 3.69 (2 H, br, NH_2), 2.77 (2 H, t, J 7.4 Hz, S-$\underline{CH_2}$-CH_2-), 1.55 (2 H, quin, J 7.4 Hz, S-CH_2-$\underline{CH_2}$-CH_2-), 1.41 (2 H, sext, J 7.4 Hz, S-CH_2-CH_2-$\underline{CH_2}$-CH_3), 0.90 (3 H, t, J 7.4 Hz, S-CH_2-CH_2-CH_2-$\underline{CH_3}$)

δ_C/ppm (100 MHz, $CDCl_3$): 145.78, 133.69, 123.76, 115.58, 36.10, 31.54, 21.85, 13.72

Data consistent with reported values [6]

4-(Pentylthio)aniline

Brown oil. Yield: 1.62 g, 34.6 %. RF: 0.38

ν_{max}/cm^{-1}: 3465, 3356, 3210, 2954, 2925, 2856, 1618, 1595, 1493, 14645, 1275, 1175, 818, 728, 624, 515

δ_H/ppm (400 MHz, $CDCl_3$): 7.23 (2 H, d, J 8.6 Hz, Ar-H), 6.61 (2 H, d, J 8.6 Hz, Ar-H), 3.68 (2H, br, NH_2), 2.76 (2 H, t, J 7.4 Hz, S-$\underline{CH_2}$-CH_2-), 1.57 (2 H, quin, J 7.4 Hz, S-CH_2-$\underline{CH_2}$-CH_2-), 1.32 (4 H, m, S-CH_2-CH_2-$\underline{CH_2}$-$\underline{CH_2}$-CH_3), 0.88 (3 H, t, J 7.2 Hz, S-CH_2-CH_2-CH_2-CH_2-$\underline{CH_3}$)

δ_C/ppm (100 MHz, $CDCl_3$): 145.69, 133.69, 123.86, 115.57, 36.39, 30.90, 29.11, 22.29, 14.01

Data consistent with reported values [7]

4-(Hexylthio)aniline

Brown oil. Yield: 2.30 g, 45.8 %. RF: 0.33

ν_{max}/cm^{-1}: 3465, 3357, 3215, 2953, 2924, 2854, 1618, 1596, 1494, 1465, 1278, 1176, 820, 724, 623, 515

δ_H/ppm (400 MHz, $CDCl_3$): 7.23 (2 H, d, J 7.9 Hz, Ar-H), 6.59 (2 H, d, J 7.9 Hz, Ar-H), 3.68 (2 H, br, NH_2), 2.76 (2 H, t, J 7.3 Hz, S-$\underline{CH_2}$-CH_2-), 1.55 (2 H, quin, J 7.3 Hz, S-CH_2-$\underline{CH_2}$-CH_2-), 1.30 (6 H, m, S-CH_2-CH_2-$\underline{CH_2}$-$\underline{CH_2}$-$\underline{CH_2}$-CH_3), 0.87 (3 H, t, J 7.0 Hz, S-CH_2-CH_2-CH_2-CH_2-CH_2-$\underline{CH_3}$)

δ_C/ppm (100 MHz, $CDCl_3$): 145.54, 133.67, 123.96, 115.55, 36.41, 31.42, 29.39, 28.40, 22.57, 14.05

Data consistent with reported values [8]

4-(Heptylthio)aniline

Brown oil. Yield: 1.23 g, 22.9 %. RF: 0.37

ν_{max}/cm^{-1}: 3465, 3356, 3208, 2953, 2924, 2853, 1619, 1596, 1494, 1465, 1276, 1176, 819, 723, 624, 514

δ_H/ppm (400 MHz, $CDCl_3$): 7.23 (2 H, d, J 8.5 Hz, Ar-H), 6.62 (2 H, d, J 8.5 Hz, Ar-H), 3.68 (2 H, br, NH_2), 2.76 (2 H, t, J 7.4 Hz, S-$\underline{CH_2}$-CH_2-), 1.56 (2 H, quin, J 7.4 Hz, S-CH_2-$\underline{CH_2}$-CH_2-), 1.29 (8 H, m, S-CH_2-CH_2-$\underline{CH_2\text{-}CH_2\text{-}CH_2\text{-}CH_2}$-$CH_3$), 0.87 (3 H, t, J 7.0 Hz, S-CH_2-CH_2-CH_2-CH_2-CH_2-CH_2-$\underline{CH_3}$)

δ_C/ppm (100 MHz, $CDCl_3$): 145.66, 133.69, 123.91, 115.56, 36.42, 31.75, 29.42, 28.88, 28.68, 22.61, 14.09

4-(Octylthio)aniline

Brown oil. Yield: 2.50 g, 43.9 %. RF: 0.33

ν_{max}/cm^{-1}: 3459, 3362, 3215, 2923, 2852, 1618, 1596, 1494, 1464, 1276, 1176, 820, 722, 623, 515

δ_H/ppm (400 MHz, $CDCl_3$): 7.23 (2 H, d, J 8.5 Hz, Ar-H), 6.62 (2 H, d, J 8.5 Hz, Ar-H), 3.67 (2 H, br, NH_2), 2.76 (2 H, t, J 7.3 Hz, S-$\underline{CH_2}$-CH_2-), 1.55 (2 H, quin, J 7.3 Hz, S-CH_2-$\underline{CH_2}$-CH_2-), 1.27 (10 H, m, S-CH_2-CH_2-$\underline{CH_2\text{-}CH_2\text{-}CH_2\text{-}CH_2\text{-}CH_2}$-$CH_3$), 0.86 (3 H, t, J 7.1 Hz, S-CH_2-CH_2-CH_2-CH_2-CH_2-CH_2-CH_2-$\underline{CH_3}$)

δ_C/ppm (100 MHz, $CDCl_3$): 145.54, 133.67, 123.97, 115.54, 36.41, 31.82, 29.41, 29.20, 29.17, 28.72, 22.65, 14.11

Data consistent with reported values [6]

4-(Nonylthio)aniline

Brown solid. Yield: 1.62 g, 26.8 %. RF: 0.37. MP: 30 °C

ν_{max}/cm^{-1}: 3465, 3362, 3212, 2923, 2852, 1619, 1597, 1494, 1465, 1278, 1176, 820, 721, 624, 515

δ_H/ppm (400 MHz, $CDCl_3$): 7.23 (2 H, d, J 8.5 Hz, Ar-H), 6.62 (2 H, d, J 8.5 Hz, Ar-H), 3.67 (2 H, br, NH_2), 2.76 (2 H, t, J 7.3 Hz, S-$\underline{CH_2}$-CH_2-), 1.55 (2 H, quin, J 7.3 Hz, S-CH_2-$\underline{CH_2}$-CH_2-), 1.25 (12 H, m, S-CH_2-CH_2-$\underline{CH_2\text{-}CH_2\text{-}CH_2\text{-}CH_2\text{-}CH_2\text{-}CH_2}$-$CH_3$), 0.88 (3 H, t, J 7.2 Hz, S-CH_2-CH_2-CH_2-CH_2-CH_2-CH_2-CH_2-CH_2-$\underline{CH_3}$)

δ_C/ppm (100 MHz, $CDCl_3$): 145.65, 133.68, 123.92, 115.55, 36.42, 31.88, 29.49, 29.42, 29.27, 29.22, 28.72, 22.68, 14.13

Data consistent with reported values [8]

4-(Decylthio)aniline

Brown solid. Yield: 0.688 g, 32.4 %. RF: 0.42. MP: 35 °C

ν_{max}/cm^{-1}: 3466, 3362, 3221, 2955, 2918, 2849, 1632, 1602, 1492, 1475, 1460, 1381, 1283, 1203, 1183, 1095, 1016, 810, 729, 717, 672, 634, 503, 485

δ_H/ppm (400 MHz, $CDCl_3$): 7.23 (2 H, d, J 7.7 Hz, Ar-H), 6.60 (2 H, d, J 7.8 Hz, Ar-H), 3.66 (2 H, br, NH_2), 2.76 (2 H, t, J 7.5 Hz, S-$\underline{CH_2}$-CH_2-), 1.56 (2 H, quin, J 7.5 Hz, S-CH_2-$\underline{CH_2}$-CH_2-), 1.25 (14 H, m, S-CH_2-CH_2-$\underline{CH_2\text{-}CH_2\text{-}CH_2\text{-}CH_2\text{-}CH_2\text{-}CH_2\text{-}CH_2}$-$CH_3$), 0.88 (3 H, t, J 7.0 Hz, S-CH_2-CH_2-CH_2-CH_2-CH_2-CH_2-CH_2-CH_2-$\underline{CH_3}$)

δ_C/ppm (100 MHz, $CDCl_3$): 145.53, 133.67, 123.97, 115.54, 36.41, 31.90, 29.56, 29.54, 29.42, 29.32, 29.21, 28.72, 22.69, 14.13

Data consistent with reported values [9]

4-(Undecylthio)aniline

Brown solid. Yield: 0.711 g, 31.8 %. RF: 0.45. MP: 39 °C

ν_{max}/cm^{-1}: 3363, 3296, 3212, 2954, 2917, 2849, 1601, 1495, 1472, 1463, 1255, 1247, 1188, 1099, 1008, 926, 857, 807, 791, 728, 718, 698, 641, 506, 496

δ_H/ppm (400 MHz, $CDCl_3$): 7.23 (2 H, d, J 8.1 Hz, Ar-H), 6.62 (2 H, d, J 8.1 Hz, Ar-H), 3.70 (2 H, br, NH_2), 2.76 (2 H, t, J 7.5 Hz, S-$\underline{CH_2}$-CH_2-), 1.56 (2 H, quin, J 7.5 Hz, S-CH_2-$\underline{CH_2}$-CH_2-), 1.25 (16 H, m, S-CH_2-CH_2-$\underline{CH_2\text{-}CH_2\text{-}CH_2\text{-}CH_2\text{-}CH_2\text{-}CH_2\text{-}CH_2}$-$CH_3$), 0.88 (3 H, t, J 7.1 Hz, S-CH_2-CH_2-CH_2-CH_2-CH_2-CH_2-CH_2-CH_2-CH_2-$\underline{CH_3}$)

δ_C/ppm (100 MHz, $CDCl_3$): 145.60, 133.67, 123.97, 115.55, 36.41, 31.92, 29.61, 29.60, 29.56, 29.42, 29.35, 29.22, 28.72, 22.70, 14.14

Data consistent with reported values [8]

4-(Dodecylthio)aniline

Brown solid. Yield: 0.967 g, 37.4 %. RF: 0.47. MP: 52 °C

ν_{max}/cm^{-1}: 3445, 3345, 2937, 2916, 2848, 1619, 1595, 1494, 1460, 1425, 1291, 1244, 1178, 1123, 828, 813, 722, 638, 518

δ_H/ppm (400 MHz, $CDCl_3$): 7.23 (2 H, d, J 8.4 Hz, Ar-H), 6.62 (2 H, d, J 8.4 Hz, Ar-H), 3.68 (2 H, br, NH_2), 2.76 (2 H, t, J 7.4 Hz, S-$\underline{CH_2}$-CH_2-), 1.55 (2 H, quin, J 7.4 Hz, S-CH_2-$\underline{CH_2}$-CH_2-), 1.25 (18 H, m, S-CH_2-CH_2-$\underline{CH_2\text{-}CH_2\text{-}CH_2\text{-}CH_2\text{-}CH_2\text{-}CH_2\text{-}CH_2\text{-}CH_2\text{-}CH_2}$-$CH_3$), 0.88 (3 H, t, J 7.3 Hz, S-CH_2-CH_2-CH_2-CH_2-CH_2-CH_2-CH_2-CH_2-CH_2-CH_2-$\underline{CH_3}$)

δ_C/ppm (100 MHz, $CDCl_3$): 145.65, 133.68, 123.93, 115.55, 36.42, 31.93, 29.66, 29.65, 29.61, 29.54, 29.42, 29.36, 29.22, 28.72, 22.70, 14.13

Data consistent with reported values [6]

4-(Tridecylthio)aniline

Brown solid. Yield: 0.943 g, 38.3 %. RF: 0.40. MP: 48 °C

ν_{max}/cm^{-1}: 3363, 3294, 3208, 2954, 2916, 2848, 1601, 1495, 1472, 1463, 1254, 1237, 1097, 1009, 926, 859, 807, 792, 78, 718, 698, 641, 506, 496

δ_H/ppm (400 MHz, $CDCl_3$): 7.23 (2 H, d, J 8.2 Hz, Ar-H), 6.61 (2 H, d, J 8.2 Hz, Ar-H), 3.66 (2 H, br, NH_2), 2.75 (2 H, t, J 7.6 Hz, S-$\underline{CH_2}$-CH_2-), 1.55 (2 H, quin, J 7.6 Hz, S-CH_2-$\underline{CH_2}$-CH_2-), 1.26 (20 H, m, S-CH_2-CH_2-$\underline{CH_2\text{-}CH_2\text{-}CH_2\text{-}CH_2\text{-}CH_2\text{-}CH_2\text{-}CH_2\text{-}CH_2\text{-}CH_2\text{-}CH_2}$-$CH_3$), 0.88 (3 H, t, J 7.0 Hz, S-CH_2-CH_2-CH_2-CH_2-CH_2-CH_2-CH_2-CH_2-CH_2-CH_2-$\underline{CH_3}$)

δ_C/ppm (100 MHz, $CDCl_3$): 145.64, 133.67, 123.92, 115.56, 36.41, 31.93, 29.68, 29.65, 29.64, 29.60, 29.54, 29.42, 29.36, 29.21, 28.72, 22.70, 14.13

Data consistent with reported values [8]

4-(Pentadecylthio)aniline

Brown solid. Yield: 0.742 g, 27.6 %. RF: 0.51. MP: 57 °C

ν_{max}/cm^{-1}: 3362, 3294, 3215, 2954, 2916, 2848, 1604, 1496, 1473, 1463, 1255, 1098, 1009, 926, 860, 807, 792, 729, 719, 698, 642, 506, 495

δ_H/ppm (400 MHz, $CDCl_3$): 7.23 (2 H, d, J 8.3 Hz, Ar-H), 6.62 (2 H, d, J 8.3 Hz, Ar-H), 3.67 (2 H, br, NH_2), 2.76 (2 H, t, J 7.4 Hz, S-$\underline{CH_2}$-CH_2-), 1.55 (2 H, m, S-CH_2-$\underline{CH_2}$-CH_2-), 1.25 (24 H, m, S-CH_2-CH_2-$\underline{CH_2\text{-}CH_2\text{-}CH_2\text{-}CH_2\text{-}CH_2\text{-}CH_2\text{-}CH_2\text{-}CH_2\text{-}CH_2\text{-}CH_2\text{-}CH_2}$-$CH_3$), 0.88 (3 H, t, J 7.1 Hz, S-CH_2-CH_2-CH_2-CH_2-CH_2-CH_2-CH_2-CH_2-CH_2-CH_2-CH_2-CH_2-$\underline{CH_3}$)

δ_C/ppm (100 MHz, $CDCl_3$): 145.64, 133.68, 123.93, 115.56, 36.42, 31.94, 29.71 (2 × C), 29.70, 29.68, 29.67, 29.61, 29.54, 29.42, 29.38, 29.22, 28.73, 22.71, 14.14

Data consistent with reported values [8]

4-(Heptadecylthio)aniline

Brown solid. Yield: 0.805 g, 27.7 %. RF: 0.57. MP: 65 °C

ν_{max}/cm^{-1}: 3361, 3294, 3212, 2954, 2916, 2848, 1602, 1496, 1473, 1463, 1255, 1098, 1009, 926, 860, 807, 792, 729, 719, 978, 642, 507, 496

δ_H/ppm (400 MHz, $CDCl_3$): 7.23 (2 H, d, J 8.5 Hz, Ar-H), 6.62 (2 H, d, J 8.5 Hz, Ar-H), 3.67 (2 H, br, NH_2), 2.76 (2 H, t, J 7.6 Hz, S-$\underline{CH_2}$-CH_2-), 1.55 (2 H, m, S-CH_2-$\underline{CH_2}$-CH_2-), 1.25 (28 H, m, S-CH_2-CH_2-$\underline{CH_2\text{-}CH_2\text{-}CH_2\text{-}CH_2\text{-}CH_2\text{-}CH_2\text{-}CH_2\text{-}CH_2\text{-}CH_2\text{-}CH_2\text{-}CH_2\text{-}CH_2\text{-}CH_2\text{-}CH_2}$-$CH_3$), 0.88 (3 H, t, J 7.0 Hz, S-CH_2-CH_2-CH_2-CH_2-CH_2-CH_2-CH_2-CH_2-CH_2-CH_2-CH_2-CH_2-CH_2-CH_2-CH_2-CH_2-$\underline{CH_3}$)

δ_C/ppm (100 MHz, $CDCl_3$): 145.64, 133.68, 123.93, 115.55, 36.42, 31.94, 29.71, 29.69 (4 × C), 29.67 (2 × C), 29.61, 29.55, 29.42, 29.38, 29.22, 28.73, 22.71, 14.14

4-(Octadecylthio)aniline

Brown solid. Yield: 1.15 g, 38.1 %. RF: 0.48. MP: 64 °C

ν_{max}/cm^{-1}: 3361, 3294, 3209, 2954, 2915, 2848, 1602, 1496, 1472, 1462, 1254, 1098, 1009, 926, 860, 807, 792, 729, 719, 692, 642, 507, 496

δ_H/ppm (400 MHz, $CDCl_3$): 7.23 (2 H, d, J 8.6 Hz, Ar-H), 6.62 (2 H, d, J 8.6 Hz, Ar-H), 3.67 (2 H, br, NH_2), 2.76 (2 H, t, J 7.4 Hz, S-$\underline{CH_2}$-CH_2-), 1.56 (2 H, quin, J 7.4 Hz, S-CH_2-$\underline{CH_2}$-CH_2-), 1.25 (30 H, m, S-CH_2-CH_2-$\underline{CH_2\text{-}CH_2\text{-}CH_2\text{-}CH_2\text{-}CH_2\text{-}CH_2\text{-}CH_2\text{-}CH_2\text{-}CH_2\text{-}CH_2\text{-}CH_2\text{-}CH_2\text{-}CH_2\text{-}CH_2}$-$CH_3$), 0.88 (3 H, t, J 7.0 Hz, S-CH_2-CH_2-CH_2-CH_2-CH_2-CH_2-CH_2-CH_2-CH_2-CH_2-CH_2-CH_2-CH_2-CH_2-CH_2-$\underline{CH_3}$)

δ_C/ppm (100 MHz, $CDCl_3$): 145.64, 133.68, 123.93, 115.55, 36.42, 31.94, 29.72, 29.69 (5 × C), 29.67 (2 × C), 29.61, 29.55, 29.43, 29.38, 29.22, 28.73, 22.71, 14.14

4-(Docosylthio)aniline

Brown solid. Yield: 0.851 g, 24.5 %. RF: 0.44. MP: 74 °C

ν_{max}/cm^{-1}: 3361, 3293, 3218, 2955, 2915, 2848, 1602, 1496, 1472, 1462, 1255, 1098, 1008, 926, 860, 807, 790, 729, 719, 691, 641, 506, 496

δ_H/ppm (400 MHz, $CDCl_3$): 7.23 (2 H, d, J 8.6 Hz, Ar-H), 6.62 (2 H, d, J 8.6 Hz, Ar-H), 3.67 (2H, br, NH_2), 2.75 (2 H, t, J 7.4 Hz, S-$\underline{CH_2}$-CH_2-), 1.55 (2 H, quin, J 7.4 Hz, S-CH_2-$\underline{CH_2}$-CH_2-), 1.25 (38 H, m, S-CH_2-CH_2-$\underline{CH_2\text{-}CH_2\text{-}CH_2\text{-}CH_2\text{-}CH_2\text{-}CH_2\text{-}CH_2\text{-}CH_2\text{-}CH_2\text{-}CH_2\text{-}CH_2\text{-}CH_2\text{-}CH_2\text{-}CH_2\text{-}CH_2\text{-}CH_2\text{-}CH_2\text{-}CH_2}$-$CH_3$), 0.88 (3 H, t, J 7.1 Hz, S-CH_2-CH_2-CH_2-CH_2-CH_2-CH_2-CH_2-CH_2-CH_2-CH_2-CH_2-CH_2-CH_2-CH_2-CH_2-CH_2-CH_2-CH_2-$\underline{CH_3}$)

δ_C/ppm (100 MHz, $CDCl_3$): 145.64, 133.68, 123.93, 115.55, 36.42, 31.94, 29.72 (10 × C), 29.67 (2 × C), 29.62, 29.55, 29.42, 29.38, 29.23, 28.73, 22.71, 14.14

SI1.2.6 4'-(6-{4-[(E)-{[4-(Alkylthio)phenyl]imino}methyl]phenoxy}hexyl)[1,1'-biphenyl]-4-carbonitriles, CB6O.S*m* series (1.6)

To a pre-dried flask flushed with argon and fitted with a condenser, compound **1.4** (1 eq, 0.200 g, 5.22×10^{-4} mol) and compound **1.5** (2 eq) of the appropriate chain length were added along with ethanol (25 mL) and the mixture was then stirred. The quantities of the 4-(alkylthio)anilines used in each reaction are listed in **Table SI1.2**. The reaction was heated to reflux and *p*-toluenesulfonic acid (catalytic amount) was then added before being left

overnight. The reaction mixture was then cooled to room temperature and while cooling a yellow or purple precipitate formed which was collected by vacuum filtration. The solid was recrystallised from hot ethanol (15 mL).

Table S 1.2. Quantities of 4-(alkylthio)anilines used in the syntheses of 4'-(6-{4-[(E)-{[4-(alkylthio)phenyl]imino}methyl]phenoxy}hexyl)[1,1'-biphenyl]-4-carbonitriles (**1.6**).

m	(**1.5**)
1	0.129 mL, 0.145 g, 1.04×10^{-3} mol
2	0.159 g, 1.04×10^{-3} mol
3	0.174 g, 1.04×10^{-3} mol
4	0.189 g, 1.04×10^{-3} mol
5	0.203 g, 1.04×10^{-3} mol
6	0.218 g, 1.04×10^{-3} mol
7	0.232 g, 1.04×10^{-3} mol
8	0.247 g, 1.04×10^{-3} mol
9	0.272 g, 1.04×10^{-3} mol
10	0.276 g, 1.04×10^{-3} mol
11	0.291 g, 1.04×10^{-3} mol
12	0.305 g, 1.04×10^{-3} mol
13	0.320 g, 1.04×10^{-3} mol
15	0.349 g, 1.04×10^{-3} mol
17	0.378 g, 1.04×10^{-3} mol
18	0.393 g, 1.04×10^{-3} mol
22	0.451 g, 1.04×10^{-3} mol

4'-(6-{4-[(E)-{[4-(Methylthio)phenyl]imino}methyl]phenoxy}hexyl)[1,1'-biphenyl]-4-carbonitrile (CB6O.S1)

Yellow solid. Yield: 0.123 g, 46.7 %

T_{Cr-} 140 °C $T_{N_{TB}N}$ (100 °C) T_{NI} (138 °C)

ν_{max}/cm^{-1}: 2924, 2853, 2224, 1604, 1569, 1509, 1489, 1395, 1306, 1246, 1194, 1167, 1108, 1090, 1045, 1014, 972, 884, 833, 817, 726, 681, 541

δ_H/ppm (400 MHz, $CDCl_3$): 8.38 (1 H, s, (C=N)-H), 7.82 (2 H, d, J 8.4 Hz, Ar-H), 7.71 (2 H, d, J 8.3 Hz, Ar-H), 7.67 (2 H, d, J 8.3 Hz, Ar-H), 7.51 (2 H, d, J 7.8 Hz, Ar-H), 7.29 (4 H, m,

Ar-H), 7.15 (2 H, d, J 8.3 Hz, Ar-H), 6.96 (2 H, d, J 8.4 Hz, Ar-H), 4.02 (2 H, t, J 6.5 Hz, O-$\underline{CH_2}$-CH_2-), 2.69 (2 H, t, J 7.6 Hz, Ar-$\underline{CH_2}$-CH_2-), 2.51 (3 H, s, S-$\underline{CH_3}$), 1.83 (2 H, tt, 6.9 Hz, 6.5 Hz, O-CH_2-$\underline{CH_2}$-CH_2-), 1.71 (2 H, quin, 7.6 Hz, Ar-CH_2-$\underline{CH_2}$-CH_2-), 1.49 (4 H, m, Ar-CH_2-CH_2-$\underline{CH_2}$-$\underline{CH_2}$-CH_2-)

δ_C/ppm (100 MHz, $CDCl_3$): 161.80, 159.12, 149.71, 145.57, 143.49, 136.55, 135.30, 132.57, 130.46, 129.19, 129.09, 127.84, 127.48, 127.12, 121.53, 119.03, 114.69, 110.58, 68.05, 35.50, 31.25, 29.09, 28.94, 25.88, 16.52

Elemental Analysis: Calculated for $C_{33}H_{32}N_2OS$: C = 78.54 %, H = 6.39 %, N = 5.55 %, S = 6.35 %; Found: C = 78.94 %, H = 6.38 %, N = 5.47 %, S = 6.15 %

4'-(6-{4-[(E)-{[4-(Ethylthio)phenyl]imino}methyl]phenoxy}hexyl)[1,1'-biphenyl]-4-carbonitrile (CB6O.S2)

Yellow solid. Yield: 0.200 g, 73.9 %

T_{Cr-} 140 °C $T_{N_{TB}N}$ (85 °C) T_{NI} (117 °C)

ν_{max}/cm^{-1}: 2829, 2854, 2225, 1603, 1569, 1507, 1493, 1462, 1396, 1308, 1247, 1195, 1168, 1108, 1091, 1050, 1006, 977, 883, 834, 726, 684, 567, 541

δ_H/ppm (400 MHz, $CDCl_3$): 8.38 (1 H, s, (C=N)-H), 7.82 (2 H, d, J 8.3 Hz, Ar-H), 7.71 (2 H, d, J 8.0 Hz, Ar-H), 7.67 (2 H, d, J 8.0 Hz, Ar-H), 7.51 (2 H, d, J 7.7 Hz, Ar-H), 7.36 (2 H, d, J 8.1 Hz, Ar-H), 7.29 (2 H, d, J 7.7 Hz, Ar-H), 7.14 (2 H, d, J 8.1 Hz, Ar-H), 6.96 (2 H, d, J 8.3 Hz, Ar-H), 4.02 (2 H, t, J 6.5 Hz, O-$\underline{CH_2}$-CH_2-), 2.95 (2 H, quart, J 7.4 Hz, S-$\underline{CH_2}$-CH_3), 2.69 (2 H, t, J 7.7 Hz, Ar-$\underline{CH_2}$-CH_2-), 1.83 (2 H, tt, 7.0 Hz, 6.5 Hz, O-CH_2-$\underline{CH_2}$-CH_2-), 1.72 (2 H, quin, 7.7 Hz, Ar-CH_2-$\underline{CH_2}$-CH_2-), 1.51 (4 H, m, Ar-CH_2-CH_2-$\underline{CH_2}$-$\underline{CH_2}$-CH_2-), 1.32 (3 H, t, J 7.4 Hz, S-CH_2-$\underline{CH_3}$)

δ_C/ppm (100 MHz, $CDCl_3$): 161.84, 159.34, 150.43, 145.57, 143.49, 136.55, 133.29, 132.57, 130.51, 130.50, 129.19, 129.05, 127.48, 127.12, 121.48, 119.04, 114.70, 110.57, 68.06, 35.51, 31.26, 29.09, 28.95, 28.39, 25.88, 14.48

Elemental Analysis: Calculated for $C_{34}H_{34}N_2OS$: C = 78.73 %, H = 6.61 %, N = 5.40 %, S = 6.18 %; Found: C = 78.84 %, H = 6.60 %, N = 5.15 %, S = 6.12 %

4'-(6-{4-[(E)-{[4-(Propylthio)phenyl]imino}methyl]phenoxy}hexyl)[1,1'-biphenyl]-4-carbonitrile (CB6O.S3)

Yellow solid. Yield: 0.149 g, 53.6 %

T_{Cr-} 131 °C T_{NI} (100 °C)

ν_{max}/cm^{-1}: 2928, 2854, 2224, 1604, 1568, 1508, 1493, 1401, 1307, 1250, 1195, 1190, 1107, 1090, 1005, 971, 882, 837, 814, 726, 687, 590, 542

δ_H/ppm (400 MHz, $CDCl_3$): 8.38 (1 H, s, (C=N)-H), 7.82 (2 H, d, J 8.1 Hz, Ar-H), 7.71 (2 H, d, J 8.0 Hz, Ar-H), 7.67 (2 H, d, J 8.0 Hz, Ar-H), 7.51 (2 H, d, J 7.6 Hz, Ar-H), 7.36 (2 H, d, J 7.9 Hz, Ar-H), 7.29 (2 H, d, J 7.6 Hz, Ar-H), 7.14 (2 H, d, J 7.9 Hz, Ar-H), 6.96 (2 H, d, J 8.1 Hz, Ar-H), 4.02 (2 H, t, J 6.4 Hz, O-$\underline{CH_2}$-CH_2-), 2.90 (2 H, t, J 7.3 Hz, S-$\underline{CH_2}$-CH_2-), 2.69 (2 H, t, J 7.6 Hz, Ar-$\underline{CH_2}$-CH_2-), 1.83 (2 H, tt, 7.2 Hz, 6.4 Hz, O-CH_2-$\underline{CH_2}$-CH_2-), 1.70 (4 H, m, Ar-CH_2-$\underline{CH_2}$-CH_2-, S-CH_2-$\underline{CH_2}$-CH_3), 1.50 (4 H, m, Ar-CH_2-CH_2-$\underline{CH_2}$-$\underline{CH_2}$-CH_2-), 1.03 (3 H, t, J 7.2 Hz, S-CH_2-CH_2-$\underline{CH_3}$)

δ_C/ppm (100 MHz, $CDCl_3$): 161.83, 159.29, 150.34, 145.57, 143.49, 136.56, 133.65, 132.57, 130.49, 130.41, 129.19, 129.07, 127.48, 127.12, 121.47, 119.03, 114.69, 110.58, 68.06, 36.36, 35.51, 31.26, 29.09, 28.95, 25.89, 22.59, 13.44

Elemental Analysis: Calculated for $C_{35}H_{36}N_2OS$: C = 78.91 %, H = 6.81 %, N = 5.26 %, S = 6.02 %; Found: C = 78.55 %, H = 6.77 %, N = 5.02 %, S = 6.18 %

4'-(6-{4-[(E)-{[4-(Butylthio)phenyl]imino}methyl]phenoxy}hexyl)[1,1'-biphenyl]-4-carbonitrile (CB6O.S4)

Yellow solid. Yield: 0.186 g, 65.2 %

T_{Cr-} 117 °C $T_{N_{TB}N}$ (73 °C) T_{NI} (101 °C)

ν_{max}/cm^{-1}: 2927, 2854, 2223, 1604, 1569, 1508, 1494, 1423, 1400, 1307, 1248, 1196, 1169, 1108, 1091, 1033, 1006, 883, 837, 816, 726, 689, 590, 562, 541

δ_H/ppm (400 MHz, $CDCl_3$): 8.37 (1 H, s, (C=N)-H), 7.81 (2 H, d, J 8.3 Hz, Ar-H), 7.70 (2 H, d, J 8.2 Hz, Ar-H), 7.66 (2 H, d, J 8.2 Hz, Ar-H), 7.50 (2 H, d, J 7.9 Hz, Ar-H), 7.35 (2 H, d, J 8.2 Hz, Ar-H), 7.29 (2 H, d, J 7.9 Hz, Ar-H), 7.13 (2 H, d, J 8.2 Hz, Ar-H), 6.95 (2 H, d, J 8.3 Hz, Ar-H), 4.02 (2 H, t, J 6.6 Hz, O-$\underline{CH_2}$-CH_2-), 2.92 (2 H, t, J 7.4 Hz, S-$\underline{CH_2}$-CH_2-), 2.69 (2 H, t, J 7.7 Hz, Ar-$\underline{CH_2}$-CH_2-), 1.82 (2 H, tt, 7.0 Hz, 6.6 Hz, O-CH_2-$\underline{CH_2}$-CH_2-), 1.67 (4 H, m, Ar-CH_2-$\underline{CH_2}$-CH_2-, S-CH_2-$\underline{CH_2}$-CH_2-), 1.47 (6 H, m, Ar-CH_2-CH_2-$\underline{CH_2}$-$\underline{CH_2}$-CH_2-, S-CH_2-CH_2-$\underline{CH_2}$-CH_3), 0.92 (3 H, t, J 7.3 Hz, S-CH_2-CH_2-CH_2-$\underline{CH_3}$)

δ_C/ppm (100 MHz, $CDCl_3$): 161.83, 159.35, 150.25, 145.57, 143.49, 136.55, 133.76, 132.57, 130.50, 130.29, 129.19, 129.03, 127.48, 127.11, 121.47, 119.03, 114.70, 110.55, 68.06, 35.50, 34.00, 31.30, 31.25, 29.08, 28.94, 25.88, 21.95, 13.67

Elemental Analysis: Calculated for $C_{36}H_{38}N_2OS$: C = 79.08 %, H = 7.01 %, N = 5.12 %, S = 5.86 %; Found: C = 79.03 %, H = 7.00 %, N = 5.00 %, S = 5.82 %

4'-(6-{4-[(E)-{[4-(Pentylthio)phenyl]imino}methyl]phenoxy}hexyl)[1,1'-biphenyl]-4-carbonitrile (CB6O.S5)

Yellow solid. Yield: 0.157 g, 53.6 %

T_{Cr-} 101 °C $T_{N_{TB}N}$ (62 °C) T_{NI} (90 °C)

ν_{max}/cm^{-1}: 2924, 2854, 2224, 1605, 1570, 1509, 1494, 1423, 1392, 1307, 1249, 1197, 1167, 1109, 1091, 1005, 884, 837, 815, 726, 687, 591, 563, 540, 521

δ_H/ppm (400 MHz, $CDCl_3$): 8.38 (1 H, s, (C=N)-H), 7.82 (2 H, d, J 8.3 Hz, Ar-H), 7.71 (2 H, d, J 8.2 Hz, Ar-H), 7.67 (2 H, d, J 8.2 Hz, Ar-H), 7.49 (2 H, d, J 7.9 Hz, Ar-H), 7.35 (2 H, d, J 8.0 Hz, Ar-H), 7.29 (2 H, d, J 7.9 Hz, Ar-H), 7.13 (2 H, d, J 8.0 Hz, Ar-H), 6.96 (2 H, d, J 8.3 Hz, Ar-H), 4.02 (2 H, t, J 6.5 Hz, O-$\underline{CH_2}$-CH_2-), 2.91 (2 H, t, J 7.4 Hz, S-$\underline{CH_2}$-CH_2-), 2.69 (2 H, t, J 7.5 Hz, Ar-$\underline{CH_2}$-CH_2-), 1.82 (2 H, tt, 7.1 Hz, 6.5 Hz, O-CH_2-$\underline{CH_2}$-CH_2-), 1.69 (4 H, m, Ar-CH_2-$\underline{CH_2}$-CH_2-, S-CH_2-$\underline{CH_2}$-CH_2-), 1.43 (8 H, m, Ar-CH_2-CH_2-$\underline{CH_2}$-$\underline{CH_2}$-CH_2-, S-CH_2-CH_2-$\underline{CH_2}$-$\underline{CH_2}$-CH_3), 0.90 (3 H, t, J 7.1 Hz, S-CH_2-CH_2-CH_2-CH_2-$\underline{CH_3}$)

δ_C/ppm (100 MHz, $CDCl_3$): 161.86, 159.37, 150.25, 145.20, 142.38, 141.47, 137.63, 137.56, 133.77, 132.64, 130.51, 130.25, 129.00, 128.98, 127.60, 127.56, 127.52, 126.93, 121.48, 118.98, 114.71, 110.82, 68.06, 35.47, 34.28, 31.30, 31.00, 29.07, 28.90, 28.89, 25.86, 22.27, 13.98

Elemental Analysis: Calculated for $C_{37}H_{40}N_2OS$: C = 79.25 %, H = 7.19 %, N = 5.00 %, S = 5.72 %; Found: C = 79.06 %, H = 7.16 %, N = 4.87 %, S = 5.88 %

4'-(6-{4-[(E)-{[4-(Hexylthio)phenyl]imino}methyl]phenoxy}hexyl)[1,1'-biphenyl]-4-carbonitrile (CB6O.S6)

Yellow solid. Yield: 0.244 g, 81.3 %

T_{Cr-} 93 °C $T_{N_{TB}N}$ (63 °C) T_{NI} (92 °C)

ν_{max}/cm^{-1}: 2921, 2853, 2230, 1606, 1572, 1510, 1494, 1461, 1423, 1391, 1306, 1254, 1196, 1162, 1107, 1090, 1000, 884, 840, 815, 749, 727, 688, 593, 561, 533, 519, 489, 459

δ_H/ppm (400 MHz, $CDCl_3$): 8.38 (1 H, s, (C=N)-H), 7.82 (2 H, d, J 8.4 Hz, Ar-H), 7.71 (2 H, d, J 8.2 Hz, Ar-H), 7.67 (2 H, d, J 8.2 Hz, Ar-H), 7.51 (2 H, d, J 7.9 Hz, Ar-H), 7.35 (2 H, d, J 8.2 Hz, Ar-H), 7.29 (2 H, d, J 7.9 Hz, Ar-H), 7.13 (2 H, d, J 8.2 Hz, Ar-H), 6.96 (2 H, d, J 8.4 Hz, Ar-H), 4.02 (2 H, t, J 6.6 Hz, O-$\underline{CH_2}$-CH_2-), 2.92 (2 H, t, J 7.5 Hz, S-$\underline{CH_2}$-CH_2-), 2.69 (2 H, t, J 7.7 Hz, Ar-$\underline{CH_2}$-CH_2-), 1.83 (2 H, tt, 7.1 Hz, 6.6 Hz, O-CH_2-$\underline{CH_2}$-CH_2-), 1.68 (4 H, m, Ar-CH_2-$\underline{CH_2}$-CH_2-, S-CH_2-$\underline{CH_2}$-CH_2-), 1.47 (6 H, m, Ar-CH_2-CH_2-$\underline{CH_2}$-$\underline{CH_2}$-CH_2-, S-CH_2-

CH_2-$\underline{CH_2}$-CH_2-), 1.29 (4 H, m, S-CH_2-CH_2-CH_2-$\underline{CH_2}$-$\underline{CH_2}$-CH_3), 0.89 (3 H, t, J 6.7 Hz, S-CH_2-CH_2-CH_2-CH_2-$\underline{CH_3}$)

δ_C/ppm (100 MHz, $CDCl_3$): 161.83, 159.29, 150.27, 145.57, 143.49, 136.55, 133.77, 132.57, 130.49, 130.28, 129.19, 129.06, 127.48, 127.12, 121.47, 119.03, 114.70, 110.57, 68.06, 35.51, 34.33, 31.39, 31.26, 29.19, 29.09, 28.95, 28.52, 25.89, 22.56, 14.05

Elemental Analysis: Calculated for $C_{38}H_{42}N_2OS$: C = 79.40 %, H = 7.36 %, N = 4.87 %, S = 5.58 %; Found: C = 78.95 %, H = 7.57 %, N = 5.02 %, S = 5.93 %

4'-(6-{4-[(E)-{[4-(Heptylthio)phenyl]imino}methyl]phenoxy}hexyl)[1,1'-biphenyl]-4-carbonitrile (CB6O.S7)

Yellow solid. Yield: 0.208 g, 67.7 %

T_{Cr-} 96 °C $T_{N_{TB}N}$ (61 °C) T_{NI} (89 °C)

ν_{max}/cm^{-1}: 2920, 2851, 2232, 1609, 1573, 1511, 1494, 1460, 1424, 1391, 1305, 1557, 1197, 1164, 1106, 1091, 1029, 1002, 886, 836, 816, 728, 688, 593, 558, 534, 519, 493

δ_H/ppm (400 MHz, $CDCl_3$): 8.38 (1 H, s, (C=N)-H), 7.82 (2 H, d, J 8.4 Hz, Ar-H), 7.71 (2 H, d, J 8.2 Hz, Ar-H), 7.67 (2 H, d, J 8.2 Hz, Ar-H), 7.50 (2 H, d, J 8.0 Hz, Ar-H), 7.35 (2 H, d, J 8.4 Hz, Ar-H), 7.29 (2 H, d, J 8.0 Hz, Ar-H), 7.13 (2 H, d, J 8.4 Hz, Ar-H), 6.96 (2 H, d, J 8.4 Hz, Ar-H), 4.02 (2 H, t, J 6.6 Hz, O-$\underline{CH_2}$-CH_2-), 2.91 (2 H, t, J 7.5 Hz, S-$\underline{CH_2}$-CH_2-), 2.69 (2 H, t, J 7.6 Hz, Ar-$\underline{CH_2}$-CH_2-), 1.83 (2 H, tt, 7.0 Hz, 6.6 Hz, O-CH_2-$\underline{CH_2}$-CH_2-), 1.69 (4 H, m, Ar-CH_2-$\underline{CH_2}$-CH_2-, S-CH_2-$\underline{CH_2}$-CH_2-), 1.47 (6 H, m, Ar-CH_2-CH_2-$\underline{CH_2}$-$\underline{CH_2}$-CH_2-, S-CH_2-CH_2-$\underline{CH_2}$-CH_2-), 1.29 (6 H, m, S-CH_2-CH_2-CH_2-$\underline{CH_2}$-CH_2-$\underline{CH_2}$-CH_3), 0.88 (3 H, t, J 6.8 Hz, S-CH_2-CH_2-CH_2-CH_2-CH_2-CH_2-$\underline{CH_3}$)

δ_C/ppm (100 MHz, $CDCl_3$): 161.83, 159.29, 150.27, 145.57, 143.49, 136.55, 133.78, 132.57, 130.49, 130.28, 129.19, 129.06, 127.48, 127.12, 121.47, 119.03, 114.69, 110.57, 68.06, 35.51, 34.33, 31.73, 31.26, 29.23, 29.09, 28.95, 28.87, 28.80, 25.89, 22.61, 14.09

Elemental Analysis: Calculated for $C_{39}H_{44}N_2OS$: C = 79.55 %, H = 7.53 %, N = 4.76 %, S = 5.44 %; Found: C = 79.60 %, H = 7.46 %, N = 4.62 %, S = 5.53 %

4'-(6-{4-[(E)-{[4-(Octylthio)phenyl]imino}methyl]phenoxy}hexyl)[1,1'-biphenyl]-4-carbonitrile (CB6O.S8)

Yellow solid. Yield: 0.171 g, 54.3 %

T_{Cr-} 98 °C $T_{N_{TB}N}$ (65 °C) T_{NI} (90 °C)

ν_{max}/cm^{-1}: 2921, 2852, 2230, 1606, 1572, 1511, 1494, 1465, 1424, 1393, 1308, 1256, 1197, 1170, 1110, 1092, 1030, 1005, 886, 833, 814, 726, 686, 592, 561, 543, 518

δ_H/ppm (400 MHz, $CDCl_3$): 8.38 (1 H, s, (C=N)-H), 7.82 (2 H, d, J 8.3 Hz, Ar-H), 7.71 (2 H, d, J 8.2 Hz, Ar-H), 7.67 (2 H, d, J 8.2 Hz, Ar-H), 7.51 (2 H, d, J 7.9 Hz, Ar-H), 7.35 (2 H, d, J 8.1 Hz, Ar-H), 7.29 (2 H, d, J 7.9 Hz, Ar-H), 7.14 (2 H, d, J 8.1 Hz, Ar-H), 6.96 (2 H, d, J 8.3 Hz, Ar-H), 4.02 (2 H, t, J 6.5 Hz, O-$\underline{CH_2}$-CH_2-), 2.91 (2 H, t, J 7.5 Hz, S-$\underline{CH_2}$-CH_2-), 2.69 (2 H, t, J 7.6 Hz, Ar-$\underline{CH_2}$-CH_2-), 1.82 (2 H, tt, 7.1 Hz, 6.6 Hz, O-CH_2-$\underline{CH_2}$-CH_2-), 1.69 (4 H, m, Ar-CH_2-$\underline{CH_2}$-CH_2-, S-CH_2-$\underline{CH_2}$-CH_2-), 1.43 (6 H, m, Ar-CH_2-CH_2-$\underline{CH_2}$-$\underline{CH_2}$-CH_2-, S-CH_2-CH_2-$\underline{CH_2}$-CH_2-), 1.28 (8 H, m, S-CH_2-CH_2-CH_2-$\underline{CH_2}$-$\underline{CH_2}$-$\underline{CH_2}$-$\underline{CH_2}$-CH_3), 0.88 (3 H, t, J 6.8 Hz, S-CH_2-CH_2-CH_2-CH_2-CH_2-CH_2-$\underline{CH_3}$)

δ_C/ppm (100 MHz, $CDCl_3$): 161.83, 159.28, 150.28, 145.57, 143.49, 136.56, 133.78, 132.57, 130.49, 130.28, 129.19, 129.07, 127.48, 127.12, 121.47, 119.03, 114.69, 110.58, 68.06, 35.51, 34.33, 31.81, 31.26, 29.22, 29.19, 29.16, 29.09, 28.95, 28.84, 25.89, 22.66, 14.12

Elemental Analysis: Calculated for $C_{45}H_{48}N_2OS$: C = 79.69 %, H = 7.69 %, N = 4.65 %, S = 5.32 %; Found: C = 79.43 %, H = 7.60 %, N = 4.55 %, S = 5.54 %

4'-(6-{4-[(E)-{[4-(Nonylthio)phenyl]imino}methyl]phenoxy}hexyl)[1,1'-biphenyl]-4-carbonitrile (CB6O.S9)

Yellow solid. Yield: 0.197 g, 61.2 %

T_{Cr-} 83 °C $T_{N_{TB}N}$ (64 °C) T_{NI} 89 °C

ν_{max}/cm^{-1}: 2921, 2852, 22230, 1605, 1570, 1508, 1494, 1464, 1423, 1393, 1308, 1248, 1194, 1169, 1110, 1090, 1006, 885, 838, 813, 726, 686, 592, 563, 542, 520

δ_H/ppm (400 MHz, $CDCl_3$): 8.38 (1 H, s, (C=N)-H), 7.82 (2 H, d, J 8.3 Hz, Ar-H), 7.71 (2 H, d, J 8.1 Hz, Ar-H), 7.67 (2 H, d, J 8.1 Hz, Ar-H), 7.51 (2 H, d, J 7.8 Hz, Ar-H), 7.35 (2 H, d, J 8.1 Hz, Ar-H), 7.29 (2 H, d, J 7.8 Hz, Ar-H), 7.13 (2 H, d, J 8.1 Hz, Ar-H), 6.96 (2 H, d, J 8.3 Hz, Ar-H), 4.02 (2 H, t, J 6.6 Hz, O-$\underline{CH_2}$-CH_2-), 2.91 (2 H, t, J 7.5 Hz, S-$\underline{CH_2}$-CH_2-), 2.69 (2 H, t, J 7.5 Hz, Ar-$\underline{CH_2}$-CH_2-), 1.82 (2 H, tt, 7.0 Hz, 6.6 Hz, O-CH_2-$\underline{CH_2}$-CH_2-), 1.66 (4 H, m, Ar-CH_2-$\underline{CH_2}$-CH_2-, S-CH_2-$\underline{CH_2}$-CH_2-), 1.48 (6 H, m, Ar-CH_2-CH_2-$\underline{CH_2}$-$\underline{CH_2}$-CH_2-, S-CH_2-CH_2-$\underline{CH_2}$-CH_2-), 1.25 (10 H, m, S-CH_2-CH_2-CH_2-$\underline{CH_2}$-$\underline{CH_2}$-$\underline{CH_2}$-$\underline{CH_2}$-$\underline{CH_2}$-CH_3), 0.88 (3 H, t, J 7.0 Hz, S-CH_2-CH_2-CH_2-CH_2-CH_2-CH_2-CH_2-CH_2-$\underline{CH_3}$)

δ_C/ppm (100 MHz, $CDCl_3$): 161.82, 159.30, 150.26, 145.57, 143.49, 135.98, 133.78, 132.57, 130.49, 130.28, 129.19, 129.05, 127.48, 127.12, 121.47, 119.15, 114.69, 110.57, 68.06, 35.51, 34.33, 31.87, 31.26, 29.48, 29.26, 29.22, 29.20, 29.08, 28.95, 28.83, 25.89, 22.68, 14.12

Elemental Analysis: Calculated for $C_{41}H_{48}N_2OS$: C = 79.83 %, H = 7.84 %, N = 4.54 %, S = 5.20 %; Found: C = 79.81 %, H = 7.84 %, N = 4.49 %, S = 5.06 %

4'-(6-{4-[(E)-{[4-(Decylthio)phenyl]imino}methyl]phenoxy}hexyl)[1,1'-biphenyl]-4-carbonitrile (CB6O.S10)

Yellow solid. Yield: 0.150 g, 45.5 %

T_{Cr-} 84 °C $T_{N_{TB}N}$ (66 °C) T_{NI} 90 °C

ν_{max}/cm^{-1}: 2922, 2851, 2227, 2922, 2851, 2227, 1605, 1570, 1509, 1494, 1465, 1425, 1394, 1306, 1248, 1194, 1169, 1107, 1090, 1007, 972, 885, 835, 812, 724, 685, 563, 541, 479

δ_H/ppm (400 MHz, $CDCl_3$): 8.37 (1 H, s, (C=N)-H), 7.81 (2 H, d, J 8.4 Hz, Ar-H), 7.70 (2 H, d, J 8.1 Hz, Ar-H), 7.66 (2 H, d, J 8.1 Hz, Ar-H), 7.50 (2 H, d, J 7.9 Hz, Ar-H), 7.34 (2 H, d, J 8.1 Hz, Ar-H), 7.29 (2 H, d, J 7.9 Hz, Ar-H), 7.13 (2 H, d, J 8.1 Hz, Ar-H), 6.95 (2 H, d, J 8.4 Hz, Ar-H), 4.02 (2 H, t, J 6.6 Hz, O-$\underline{CH_2}$-CH_2-), 2.91 (2 H, t, J 7.4 Hz, S-$\underline{CH_2}$-CH_2-), 2.68 (2 H, t, J 7.5 Hz, Ar-$\underline{CH_2}$-CH_2-), 1.82 (2 H, tt, 7.1 Hz, 6.6 Hz, O-CH_2-$\underline{CH_2}$-CH_2-), 1.67 (4 H, m, Ar-CH_2-$\underline{CH_2}$-CH_2-, S-CH_2-$\underline{CH_2}$-CH_2-), 1.47 (6 H, m, Ar-CH_2-CH_2-$\underline{CH_2}$-$\underline{CH_2}$-CH_2-, S-CH_2-CH_2-$\underline{CH_2}$-CH_2-), 1.28 (12 H, m, S-CH_2-CH_2-CH_2-$\underline{CH_2}$-$\underline{CH_2}$-$\underline{CH_2}$-$\underline{CH_2}$-$\underline{CH_2}$-CH_2-CH_3), 0.87 (3 H, t, J 7.0 Hz, S-CH_2-CH_2-CH_2-CH_2-CH_2-CH_2-CH_2-CH_2-$\underline{CH_3}$)

δ_C/ppm (100 MHz, $CDCl_3$): 161.83, 159.36, 150.22, 145.58, 143.49, 136.55, 133.57, 132.57, 130.50, 130.27, 129.18, 129.02, 127.48, 127.11, 121.47, 119.01, 114.70, 110.54, 68.06, 35.50, 34.32, 31.90, 31.25, 29.55, 29.52, 29.31, 29.21, 29.19, 29.08, 28.94, 28.83, 25.88, 22.68, 14.12

Elemental Analysis: Calculated for $C_{42}H_{50}N_2OS$: C = 79.95 %, H = 7.99 %, N = 4.44 %, S = 5.08 %; Found: C = 79.80 %, H = 8.03 %, N = 4.43 %, S = 4.90 %

4'-(6-{4-[(E)-{[4-(Undecylthio)phenyl]imino}methyl]phenoxy}hexyl)[1,1'-biphenyl]-4-carbonitrile (CB6O.S11)

Yellow solid. Yield: 0.183 g, 54.4 %

T_{Cr-} 89 °C $T_{N_{TB}N}$ (64 °C) T_{NI} (86 °C)

ν_{max}/cm^{-1}: 2920, 2850, 2229, 1606, 1574, 1510, 1494, 1466, 1394, 1305, 1249, 1198, 1170, 1106, 1008, 971, 887, 812, 722, 684, 564, 541, 523, 478

δ_H/ppm (400 MHz, $CDCl_3$): 8.38 (1 H, s, (C=N)-H), 7.82 (2 H, d, J 8.3 Hz, Ar-H), 7.71 (2 H, d, J 8.1 Hz, Ar-H), 7.67 (2 H, d, J 8.1 Hz, Ar-H), 7.51 (2 H, d, J 7.8 Hz, Ar-H), 7.35 (2 H, d, J 8.2 Hz, Ar-H), 7.29 (2 H, d, J 7.8 Hz, Ar-H), 7.13 (2 H, d, J 8.2 Hz, Ar-H), 6.96 (2 H, d, J 8.3 Hz, Ar-H), 4.02 (2 H, t, J 6.5 Hz, O-$\underline{CH_2}$-CH_2-), 2.91 (2 H, t, J 7.4 Hz, S-$\underline{CH_2}$-CH_2-), 2.69 (2

H, t, J 7.7 Hz, Ar-$\underline{CH_2}$-CH_2-), 1.83 (2 H, tt, 7.1 Hz, 6.5 Hz, O-CH_2-$\underline{CH_2}$-CH_2-), 1.67 (4 H, m, Ar-CH_2-$\underline{CH_2}$-CH_2-, S-CH_2-$\underline{CH_2}$-CH_2-), 1.48 (6 H, m, Ar-CH_2-CH_2-$\underline{CH_2}$-$\underline{CH_2}$-CH_2-, S-CH_2-CH_2-$\underline{CH_2}$-CH_2-), 1.27 (14 H, m, S-CH_2-CH_2-CH_2-$\underline{CH_2}$-$\underline{CH_2}$-$\underline{CH_2}$-$\underline{CH_2}$-$\underline{CH_2}$-$\underline{CH_2}$-CH_3), 0.88 (3 H, t, J 6.9 Hz, S-CH_2-CH_2-CH_2-CH_2-CH_2-CH_2-CH_2-CH_2-CH_2-$\underline{CH_3}$)

δ_C/ppm (100 MHz, $CDCl_3$): 161.82, 159.26, 150.28, 145.57, 143.49, 136.56, 133.77, 132.57, 130.48, 130.28, 129.19, 129.07, 127.48, 127.12, 121.47, 119.03, 114.69, 110.58, 68.06, 35.51, 34.33, 31.92, 31.26, 29.61, 29.60, 29.52, 29.35, 29.22, 29.20, 29.09, 28.95, 28.84, 25.89, 22.70, 14.14

Elemental Analysis: Calculated for $C_{43}H_{52}N_2OS$: C = 80.08 %, H = 8.13 %, N = 4.34 %, S = 4.97 %; Found: C = 80.06 %, H = 8.24 %, N = 4.60 %, S = 4.84 %

4'-(6-{4-[(E)-{[4-(Dodecylthio)phenyl]imino}methyl]phenoxy}hexyl)[1,1'-biphenyl]-4-carbonitrile (CB6O.S12)

Purple solid. Yield: 0.215 g, 62.5 %

T_{Cr-} 90 °C T_{SmA_BN} (66 °C) T_{NI} (87 °C)

ν_{max}/cm^{-1}: 2919, 2850, 2231, 1620, 1606, 1574, 1510, 1494, 1466, 1394, 1305, 1249, 1199, 1170, 1105, 1093, 1008, 971, 888, 812, 722, 683, 564, 542, 522

δ_H/ppm (400 MHz, $CDCl_3$): 8.38 (1 H, s, (C=N)-H), 7.82 (2 H, d, J 8.7 Hz, Ar-H), 7.71 (2 H, d, J 8.5 Hz, Ar-H), 7.67 (2 H, d, J 8.5 Hz, Ar-H), 7.51 (2 H, d, J 8.2 Hz, Ar-H), 7.36 (2 H, d, J 8.5 Hz, Ar-H), 7.30 (2 H, d, J 8.2 Hz, Ar-H), 7.14 (2 H, d, J 8.5 Hz, Ar-H), 6.96 (2 H, d, J 8.7 Hz, Ar-H), 4.02 (2 H, t, J 6.5 Hz, O-$\underline{CH_2}$-CH_2-), 2.91 (2 H, t, J 7.4 Hz, S-$\underline{CH_2}$-CH_2-), 2.69 (2 H, t, J 7.5 Hz, Ar-$\underline{CH_2}$-CH_2-), 1.83 (2 H, tt, 6.9 Hz, 6.5 Hz, O-CH_2-$\underline{CH_2}$-CH_2-), 1.68 (4 H, m, Ar-CH_2-$\underline{CH_2}$-CH_2-, S-CH_2-$\underline{CH_2}$-CH_2-), 1.49 (6 H, m, Ar-CH_2-CH_2-$\underline{CH_2}$-$\underline{CH_2}$-CH_2-, S-CH_2-CH_2-$\underline{CH_2}$-CH_2-), 1.26 (16 H, m, S-CH_2-CH_2-CH_2-$\underline{CH_2}$-$\underline{CH_2}$-$\underline{CH_2}$-$\underline{CH_2}$-$\underline{CH_2}$-$\underline{CH_2}$-$\underline{CH_2}$-CH_3), 0.88 (3 H, t, J 6.9 Hz, S-CH_2-CH_2-CH_2-CH_2-CH_2-CH_2-CH_2-CH_2-CH_2-CH_2-$\underline{CH_3}$)

δ_C/ppm (100 MHz, $CDCl_3$): 161.82, 159.26, 150.28, 145.57, 143.49, 136.56, 133.78, 132.57, 130.48, 130.28, 129.19, 129.07, 127.48, 127.12, 121.47, 119.03, 114.69, 110.58, 68.06, 35.51, 34.33, 31.93, 31.26, 29.66, 29.65, 29.60, 29.53, 29.36, 29.22, 29.20, 29.09, 28.95, 28.84, 25.89, 22.71, 14.14

Elemental Analysis: Calculated for $C_{44}H_{54}N_2OS$: C = 80.20 %, H = 8.26 %, N = 4.25 %, S = 4.87 %; Found: C = 80.47 %, H = 8.26 %, N = 4.09 %, S = 4.72 %

4'-(6-{4-[(E)-{[4-(Tridecylthio)phenyl]imino}methyl]phenoxy}hexyl)[1,1'-biphenyl]-4-carbonitrile (CB6O.S13)

Yellow solid. Yield: 0.115 g, 32.7 %

T_{Cr-} 94 °C $T_{SmC_{TB}SmA_B}$ (66 °C) T_{SmA_BSmA} (66 °C) T_{SmAN} (68 °C) T_{NI} (84 °C)

ν_{max}/cm^{-1}: 2919, 2850, 2229, 1606, 1574, 1510, 1495, 1466, 1394, 1305, 1249, 1199, 1170, 1105, 1007, 971, 888, 812, 722, 684, 564, 542, 523, 480

δ_H/ppm (400 MHz, $CDCl_3$): 8.37 (1 H, s, (C=N)-H), 7.81 (2 H, d, J 8.1 Hz, Ar-H), 7.70 (2 H, d, J 7.9 Hz, Ar-H), 7.66 (2 H, d, J 7.9 Hz, Ar-H), 7.50 (2 H, d, J 7.6 Hz, Ar-H), 7.34 (2 H, d, J 7.8 Hz, Ar-H), 7.29 (2 H, d, J 7.5 Hz, Ar-H), 7.13 (2 H, d, J 7.8 Hz, Ar-H), 6.95 (2 H, d, J 8.1 Hz, Ar-H), 4.02 (2 H, t, J 6.5 Hz, O-$\underline{CH_2}$-CH_2-), 2.91 (2 H, t, J 7.2 Hz, S-$\underline{CH_2}$-CH_2-), 2.68 (2 H, t, J 7.5 Hz, Ar-$\underline{CH_2}$-CH_2-), 1.81 (2 H, tt, 7.1 Hz, 6.5 Hz, O-CH_2-$\underline{CH_2}$-CH_2-), 1.69 (4 H, m, Ar-CH_2-$\underline{CH_2}$-CH_2-, S-CH_2-$\underline{CH_2}$-CH_2-), 1.48 (6 H, m, Ar-CH_2-CH_2-$\underline{CH_2}$-$\underline{CH_2}$-CH_2-, S-CH_2-CH_2-$\underline{CH_2}$-CH_2-), 1.27 (18 H, m, S-CH_2-CH_2-CH_2-$\underline{CH_2}$-$\underline{CH_2}$-$\underline{CH_2}$-$\underline{CH_2}$-$\underline{CH_2}$-$\underline{CH_2}$-$\underline{CH_2}$-$\underline{CH_2}$-CH_3), 0.87 (3 H, t, J 7.0 Hz, S-CH_2-CH_2-CH_2-CH_2-CH_2-CH_2-CH_2-CH_2-CH_2-$\underline{CH_3}$)

δ_C/ppm (100 MHz, $CDCl_3$): 161.84, 159.39, 150.21, 145.58, 143.49, 136.54, 133.81, 132.57, 130.51, 130.27, 129.19, 129.00, 127.48, 127.11, 121.47, 119.03, 114.70, 110.53, 68.06, 35.50, 34.31, 31.93, 31.25, 29.68, 29.65, 29.64, 29.60, 29.52, 29.36, 29.21, 29.19, 29.08, 28.94, 28.83, 25.88, 22.70, 14.13

Elemental Analysis: Calculated for $C_{45}H_{56}N_2OS$: C = 80.31 %, H = 8.39 %, N = 4.16 %, S = 4.76 %; Found: C = 80.32 %, H = 8.30 %, N = 4.20 %, S = 4.51 %

4'-(6-{4-[(E)-{[4-(Pentadecylthio)phenyl]imino}methyl]phenoxy}hexyl)[1,1'-biphenyl]-4-carbonitrile (CB6O.S15)

Purple solid. Yield: 0.260 g, 71.0 %

T_{Cr-} 97 °C $T_{SmC_{TB}SmA_B}$ (72 °C) T_{SmA_BSmA} (76 °C) T_{SmAN} (78 °C) T_{NI} (84 °C)

ν_{max}/cm^{-1}: 2918, 2850, 2230, 1606, 1575, 1510, 1495, 1466, 1394, 1305, 1249, 1198, 1170, 1105, 1007, 971, 888, 813, 722, 684, 564, 542, 522, 481

δ_H/ppm (400 MHz, $CDCl_3$): 8.38 (1 H, s, (C=N)-H), 7.82 (2 H, d, J 8.4 Hz, Ar-H), 7.71 (2 H, d, J 8.2 Hz, Ar-H), 7.67 (2 H, d, J 8.2 Hz, Ar-H), 7.51 (2 H, d, J 8.0 Hz, Ar-H), 7.35 (2 H, d, J 8.5 Hz, Ar-H), 7.30 (2 H, d, J 8.0 Hz, Ar-H), 7.15 (2 H, d, J 8.5 Hz, Ar-H), 6.96 (2 H, d, J 8.4 Hz, Ar-H), 4.02 (2 H, t, J 6.5 Hz, O-$\underline{CH_2}$-CH_2-), 2.91 (2 H, t, J 7.4 Hz, S-$\underline{CH_2}$-CH_2-), 2.69 (2 H, t, J 7.7 Hz, Ar-$\underline{CH_2}$-CH_2-), 1.83 (2 H, tt, 7.0 Hz, 6.5 Hz, O-CH_2-$\underline{CH_2}$-CH_2-), 1.68 (4 H, m, Ar-CH_2-$\underline{CH_2}$-CH_2-, S-CH_2-$\underline{CH_2}$-CH_2-), 1.48 (6 H, m, Ar-CH_2-CH_2-$\underline{CH_2}$-$\underline{CH_2}$-CH_2-, S-CH_2-

CH_2-$\underline{CH_2}$-CH_2-), 1.26 (22 H, m, S-CH_2-CH_2-CH_2-$\underline{CH_2}$-$\underline{CH_2}$-$\underline{CH_2}$-$\underline{CH_2}$-$\underline{CH_2}$-$\underline{CH_2}$-$\underline{CH_2}$-$\underline{CH_2}$-$\underline{CH_2}$-$\underline{CH_2}$-CH_3), 0.88 (3 H, t, J 7.0 Hz, S-CH_2-CH_2-CH_2-CH_2-CH_2-CH_2-CH_2-CH_2-CH_2-CH_2-CH_2-CH_2-CH_2-$\underline{CH_3}$)

δ_C/ppm (100 MHz, $CDCl_3$): 161.83, 159.26, 150.26, 145.57, 143.49, 136.56, 133.78, 132.57, 130.49, 130.28, 129.19, 129.06, 127.48, 127.12, 121.47, 119.03, 114.69, 110.58, 68.06, 35.51, 34.33, 31.94, 31.26, 29.71 (2 × C), 29.70, 29.67 (2 × C), 29.61, 29.53, 29.38, 29.22, 29.20, 29.09, 28.95, 28.84, 25.89, 22.71, 14.14

Elemental Analysis: Calculated for $C_{47}H_{60}N_2OS$: C = 80.52 %, H = 8.63 %, N = 4.00 %, S = 4.57 %; Found: C = 80.54 %, H = 8.66 %, N = 4.14 %, S = 4.52 %

4'-(6-{4-[(E)-{[4-(Heptadecylthio)phenyl]imino}methyl]phenoxy}hexyl)[1,1'-biphenyl]-4-carbonitrile (CB6O.S17)

Purple solid. Yield: 0.161 g, 42.3 %

T_{Cr-} 100 °C $T_{SmC_{TB}SmA_B}$ (78 °C) T_{SmA_BSmA} (82 °C) T_{SmAN} (85 °C) T_{NI} (86 °C)

ν_{max}/cm^{-1}: 2918, 2849, 2230, 1621, 1606, 1575, 1511, 1495, 1466, 1394, 1303, 1250, 1199, 1171, 1105, 1053, 1008, 971, 890, 813, 722, 689, 564, 542, 523, 479

δ_H/ppm (400 MHz, $CDCl_3$): 8.38 (1 H, s, (C=N)-H), 7.82 (2 H, d, J 8.7 Hz, Ar-H), 7.71 (2 H, d, J 8.5 Hz, Ar-H), 7.67 (2 H, d, J 8.5 Hz, Ar-H), 7.49 (2 H, d, J 8.1 Hz, Ar-H), 7.35 (2 H, d, J 8.4 Hz, Ar-H), 7.30 (2 H, d, J 8.1 Hz, Ar-H), 7.14 (2 H, d, J 8.4 Hz, Ar-H), 6.96 (2 H, d, J 8.7 Hz, Ar-H), 4.02 (2 H, t, J 6.4 Hz, O-$\underline{CH_2}$-CH_2-), 2.91 (2 H, t, J 7.4 Hz, S-$\underline{CH_2}$-CH_2-), 2.69 (2 H, t, J 7.7 Hz, Ar-$\underline{CH_2}$-CH_2-), 1.83 (2 H, tt, 6.9 Hz, 6.4 Hz, O-CH_2-$\underline{CH_2}$-CH_2-), 1.68 (4 H, m, Ar-CH_2-$\underline{CH_2}$-CH_2-, S-CH_2-$\underline{CH_2}$-CH_2-), 1.47 (6 H, m, Ar-CH_2-CH_2-$\underline{CH_2}$-$\underline{CH_2}$-CH_2-, S-CH_2-CH_2-$\underline{CH_2}$-CH_2-), 1.25 (26 H, m, S-CH_2-CH_2-CH_2-$\underline{CH_2}$-$\underline{CH_2}$-$\underline{CH_2}$-$\underline{CH_2}$-$\underline{CH_2}$-$\underline{CH_2}$-$\underline{CH_2}$-$\underline{CH_2}$-$\underline{CH_2}$-$\underline{CH_2}$-$\underline{CH_2}$-$\underline{CH_2}$-CH_3), 0.88 (3 H, t, J 7.1 Hz, S-CH_2-CH_2-CH_2-CH_2-CH_2-CH_2-CH_2-CH_2-CH_2-CH_2-CH_2-CH_2-CH_2-CH_2-CH_2-$\underline{CH_3}$)

δ_C/ppm (100 MHz, $CDCl_3$): 161.83, 159.26, 150.25, 145.57, 143.49, 136.55, 133.80, 132.57, 130.50, 130.27, 129.19, 129.06, 127.48, 127.12, 121.47, 119.03, 114.69, 110.58, 68.06, 35.51, 34.33, 31.95, 31.26, 29.72 (4 × C), 29.70, 29.68 (2 × C), 29.61, 29.53, 29.38, 29.22, 29.20, 29.10, 28.96, 28.84, 25.89, 22.71, 14.15

Elemental Analysis: Calculated for $C_{49}H_{64}N_2OS$: C = 80.72 %, H = 8.85 %, N = 3.84 %, S = 4.40 %; Found: C = 80.73 %, H = 8.95 %, N = 3.78 %, S = 4.35 %

4'-(6-{4-[(E)-{[4-(Octadecylthio)phenyl]imino}methyl]phenoxy}hexyl)[1,1'-biphenyl]-4-carbonitrile (CB6O.S18)

Purple solid. Yield: 0.142 g, 35.9 %

T_{Cr-} 99 °C $T_{SmC_{TB}SmA_B}$ (80 °C) T_{SmA_BSmA} (83 °C) T_{SmAI} (87 °C)

ν_{max}/cm^{-1}: 2917, 2849, 2231, 1621, 1606, 1575, 1511, 1495, 1466, 1394, 1304, 1250, 1199, 1171, 1105, 1053, 1008, 971, 889, 813, 721, 684, 565, 542, 523, 478

δ_H/ppm (400 MHz, $CDCl_3$): 8.38 (1 H, s, (C=N)-H), 7.82 (2 H, d, J 8.7 Hz, Ar-H), 7.71 (2 H, d, J 8.6 Hz, Ar-H), 7.67 (2 H, d, J 8.6 Hz, Ar-H), 7.51 (2 H, d, J 8.1 Hz, Ar-H), 7.35 (2 H, d, J 8.5 Hz, Ar-H), 7.29 (2 H, d, J 8.1 Hz, Ar-H), 7.14 (2 H, d, J 8.5 Hz, Ar-H), 6.96 (2 H, d, J 8.7 Hz, Ar-H), 4.02 (2 H, t, J 6.5 Hz, O-$\underline{CH_2}$-CH_2-), 2.91 (2 H, t, J 7.4 Hz, S-$\underline{CH_2}$-CH_2-), 2.69 (2 H, t, J 7.7 Hz, Ar-$\underline{CH_2}$-CH_2-), 1.82 (2 H, tt, 6.9 Hz, 6.5 Hz, O-CH_2-$\underline{CH_2}$-CH_2-), 1.68 (4 H, m, Ar-CH_2-$\underline{CH_2}$-CH_2-, S-CH_2-$\underline{CH_2}$-CH_2-), 1.49 (6 H, m, Ar-CH_2-CH_2-$\underline{CH_2}$-$\underline{CH_2}$-CH_2-, S-CH_2-CH_2-$\underline{CH_2}$-CH_2-), 1.25 (28 H, m, S-CH_2-CH_2-CH_2-$\underline{CH_2}$-$\underline{CH_2}$-$\underline{CH_2}$-$\underline{CH_2}$-$\underline{CH_2}$-$\underline{CH_2}$-$\underline{CH_2}$-$\underline{CH_2}$-$\underline{CH_2}$-$\underline{CH_2}$-$\underline{CH_2}$-$\underline{CH_2}$-$\underline{CH_2}$-$\underline{CH_2}$-$\underline{CH_2}$-CH_3), 0.88 (3 H, t, J 7.1 Hz, S-CH_2-CH_2-CH_2-CH_2-CH_2-CH_2-CH_2-CH_2-CH_2-CH_2-CH_2-CH_2-CH_2-CH_2-CH_2-CH_2-$\underline{CH_3}$)

δ_C/ppm (100 MHz, $CDCl_3$): 161.83, 159.25, 150.26, 145.57, 143.49, 136.56, 133.79, 132.57, 130.49, 130.27, 129.19, 129.07, 127.48, 127.12, 121.47, 119.03, 114.69, 110.58, 68.06, 35.51, 34.33, 31.94, 31.26, 29.72 (5 × C), 29.70, 29.67 (2 × C), 29.61, 29.53, 29.38, 29.22, 29.20, 29.09, 28.95, 28.84, 25.89, 22.71, 14.14

Elemental Analysis: Calculated for $C_{50}H_{66}N_2OS$: C = 80.81 %, H = 8.95 %, N = 3.77 %, S = 4.31 %; Found: C = 81.03 %, H = 9.04 %, N = 3.64 %, S = 4.46 %

4'-(6-{4-[(E)-{[4-(Docsylthio)phenyl]imino}methyl]phenoxy}hexyl)[1,1'-biphenyl]-4-carbonitrile (CB6O.S22)

Purple solid. Yield: 0.168 g, 40.3 %

T_{Cr-} 103 °C T_{SmAI} (90 °C)

ν_{max}/cm^{-1}: 2917, 2849, 2231, 621, 1607, 1575, 1510, 1495, 1466, 1394, 1303, 1250, 1199, 1171, 1105, 1053, 1008, 971, 889, 813, 721, 689, 564, 542, 523, 478

δ_H/ppm (400 MHz, $CDCl_3$): 8.38 (1 H, s, (C=N)-H), 7.82 (2 H, d, J 8.8 Hz, Ar-H), 7.71 (2 H, d, J 8.6 Hz, Ar-H), 7.67 (2 H, d, J 8.6 Hz, Ar-H), 7.51 (2 H, d, J 8.2 Hz, Ar-H), 7.35 (2 H, d, J 8.5 Hz, Ar-H), 7.29 (2 H, d, J 8.2 Hz, Ar-H), 7.14 (2 H, d, J 8.5 Hz, Ar-H), 6.96 (2 H, d, J 8.8 Hz, Ar-H), 4.02 (2 H, t, J 6.5 Hz, O-$\underline{CH_2}$-CH_2-), 2.91 (2 H, t, J 7.3 Hz, S-$\underline{CH_2}$-CH_2-), 2.69 (2 H, t, J 7.6 Hz, Ar-$\underline{CH_2}$-CH_2-), 1.82 (2 H, tt, 7.0 Hz, 6.5 Hz, O-CH_2-$\underline{CH_2}$-CH_2-), 1.68 (4 H, m,

Ar-CH_2-$\underline{CH_2}$-CH_2-, S-CH_2-$\underline{CH_2}$-CH_2-), 1.46 (6 H, m, Ar-CH_2-CH_2-$\underline{CH_2}$-$\underline{CH_2}$-CH_2-, S-CH_2-CH_2-$\underline{CH_2}$-CH_2-), 1.26 (36 H, m, S-CH_2-CH_2-CH_2-$\underline{CH_2}$-$\underline{CH_2}$-$\underline{CH_2}$-$\underline{CH_2}$-$\underline{CH_2}$-$\underline{CH_2}$-$\underline{CH_2}$-$\underline{CH_2}$-$\underline{CH_2}$-$\underline{CH_2}$-$\underline{CH_2}$-$\underline{CH_2}$-$\underline{CH_2}$-$\underline{CH_2}$-$\underline{CH_2}$-$\underline{CH_2}$-CH_3), 0.88 (3 H, t, J 6.9 Hz, S-CH_2-CH_2-CH_2-CH_2-CH_2-CH_2-CH_2-CH_2-CH_2-CH_2-CH_2-CH_2-CH_2-CH_2-CH_2-CH_2-CH_2-CH_2-CH_2-CH_2-CH_2-CH_2-CH_2-CH_2-$\underline{CH_3}$)

δ_C/ppm (100 MHz, $CDCl_3$): 161.83, 159.25, 150.25, 145.57, 143.49, 136.56, 133.80, 132.57, 130.50, 130.27, 129.19, 129.06, 127.48, 127.11, 121.47, 119.03, 114.69, 110.58, 68.06, 35.51, 34.33, 31.94, 31.26, 29.72 (10 × C), 29.68 (2 × C), 29.61, 29.53, 29.38, 29.22, 29.20, 29.09, 28.96, 28.84, 25.89, 22.71, 14.14

Elemental Analysis: Calculated for $C_{54}H_{74}N_2OS$: C = 81.15 %, H = 9.33 %, N = 3.50 %, S = 4.01 %; Found: C = 81.38 %, H = 9.46 %, N = 3.34 %, S = 4.03 %

Table S2. The transition temperatures of the CB6O.S*m* series. The scaled entropy changes (ΔS/R) for each transition are given in brackets below the transition temperature. Data have been extracted from heating traces unless noted otherwise.

m	T_{Cr-}/ °C	$T_{SmC_{TB}SmA_B}$/ °C	T_{SmA_BSmA}/ °C	$T_{N_{TB}N}$/ °C *T_{SmAN}/ °C	T_{NI}/ °C *T_{SmAI}/ °C
1	140 (10.6)	-	-	[c]100	[a]138 (0.29)
2	140 (9.94)	-	-	[c]85	[a]117 [b](-)
3	131 (10.3)	-	-	[d]70	[c]100
4	117 (14.9)	-	-	[c]73	[a]101 (0.15)
5	101 (13.0)	-	-	[c]62	[a]90 (0.14)
6	93 (15.1)	-	-	[c]63	[a]92 (0.22)
7	96 (12.5)	-	-	[c]61	[a]89 (0.20)
8	98 (19.1)	-	-	[c]65	[a]90 (0.15)
9	83 (8.31)	-	-	[a]64 (0.053)	89 (0.16)
10	84 (9.26)	-	-	[a]66 [b](-)	90 (0.17)
11	89 (13.3)	-	-	[a]64 (0.030)	[a]86 (0.18)
12	90 (19.0)	-	-	[a]*66 (0.21)	[a]87 (0.33)
13	94 (18.0)	[c]65.8	[a]66 [b](-)	[a]*68 [b](-)	[a]84 (0.18)
15	97 (21.8)	[c]72	[a]76 [b](-)	[a]*78 [b](-)	[a]84 (0.30)
17	100 (23.3)	[c]78	[a]82 (0.19)	[a]*85 [b](-)	[a]86 [b](-)
18	99 (21.2)	[c]80	[a]83 [b](-)	-	[a]*87 [b](-)
22	103 (21.6)	-	-	-	[a]*90 [b](-)

[a] Values extracted from DSC cooling traces.
[b] Overlapping peaks.
[c] Measured using the polarised light microscope.
[d] Virtual transition temperatures estimated from binary phase diagram with CB7CB.

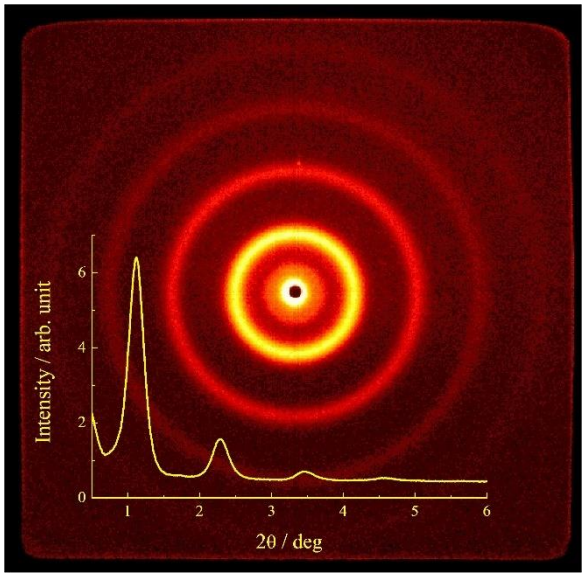

Figure S1. Low angle XRD pattern for the B_4 phase of compound CB6O.S17 measured at room temperature.

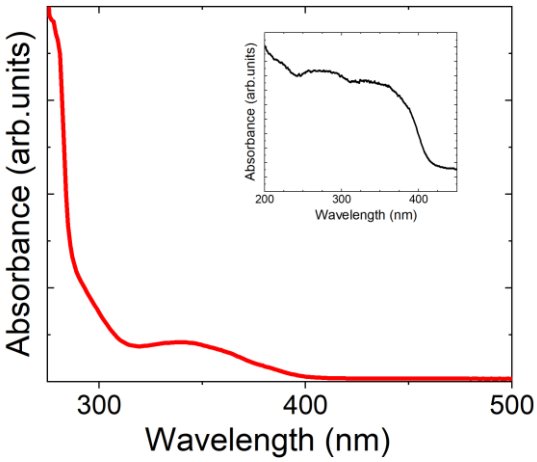

Figure S2. UV-VIS absorption spectrum measured in toluene solution of CB6O.S18. In the inset, the UV-VIS spectrum recorded in the solid state - a monodomain of B_4 phase grown on a fused quartz slide.

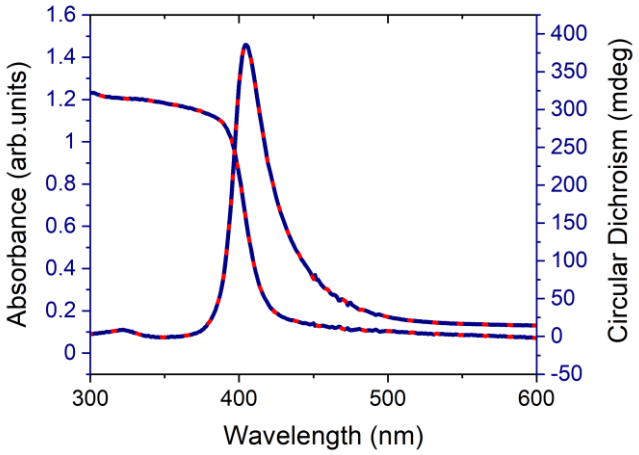

Figure S3 Circular dichroism measured simultaneously with UV-VIS spectrum. A thin film of big levo-oriented monodomain is measured on quartz in two sample orientations (red dots and navy line) – sample was rotated by 180 deg. As the signal does not change upon sample rotation it is clear there is no influence of linear birefringence on measured CD.

S2 Single crystal X-ray measurements for CB6O.S1 and CB6O.S2

The largest available single crystal specimens of **CB6O.S1** and **CB6O.S2**. were mounted on a kapton loop with a drop of ParatoneN oil. Intensity data from single crystal X-ray diffraction were measured on Rigaku Oxford Diffraction Supernova 4 circle diffractometer equipped with copper (CuKα) microsource and Atlas CCD detector at 100K. The temperature of the sample was controlled with a precision of ± 0.1 K using Oxford Cryosystems cooling device. Single crystal specimens (plates no thicker than 0.02 mm) were mounted on small kapton loops with a tiny amount of Paratone N oil. The data were collected and integrated with CrysAlis171[10] software. Data were further corrected for absorption effects using the multi-scan method (SCALE3 ABSPACK[10]). Notably, the diffractometer malfunctioned at the end of data collection for **CB6O.S1** which led to incomplete data set.

In both instances, scattering power of the mounted crystals was limited and traces of additional crystal domains could be detected, which resulted in higher R-factors and relatively large atomic displacement parameters. In the case of **CB6O.S2** elongated atomic displacement parameters also illustrate the ability of the molecules to shift in the crystal lattice along their long axis.

The structures were solved by direct methods using SXELXS[11] and refined by full-matrix least squares procedure with SHELXL[12] within OLEX2[13] graphical interface.

The most important crystallographic parameters are collected in Table SI3.

Table S3. Summary data processing, structure solution and structure refinement by single-crystal X-ray diffraction.

Structure	**CB6O.S1**	**CB6O.S2**
Empirical formula	C_{33} H_{32} N_2 O S	C_{34} H_{40} N_2 O S
Formula weight	504.66	18.69
Crystal system	triclinic	orthorhombic
Space group	P -1	P n a 21
a/Å	9.8063(6)	9.7899(8)
b/Å	11.0018(6)	9.4403(11)
c/Å	25.9498(14)	30.382(4)
α/°	94.359(4)	90
β/°	92.138(5)	90
γ/°	106.211(5)	90
Volume/Å^3	2675.5(3)	2807.9(5)
Z	4	4
Crystal size/mm	0.20	0.25
	0.12	0.15
	0.02	0.11
Rint	0.0435	0.0679

Independent reflections	8588	5131
Largest diff. peak / hole /e Å^{-3}	0.88	0.41
	-2.24	-0.27
Goodness-of-fit on F^2	2.08	1.11
R1 [I>=2σ (I)]	0.1681	0.1089
wR2 [I>=2σ (I)]	0.5471	0.2471

The structures were deposited with CCDC (deposition numbers 2077654 and 2077655 accordingly) and can be retrieved upon request.

CB6O.S1

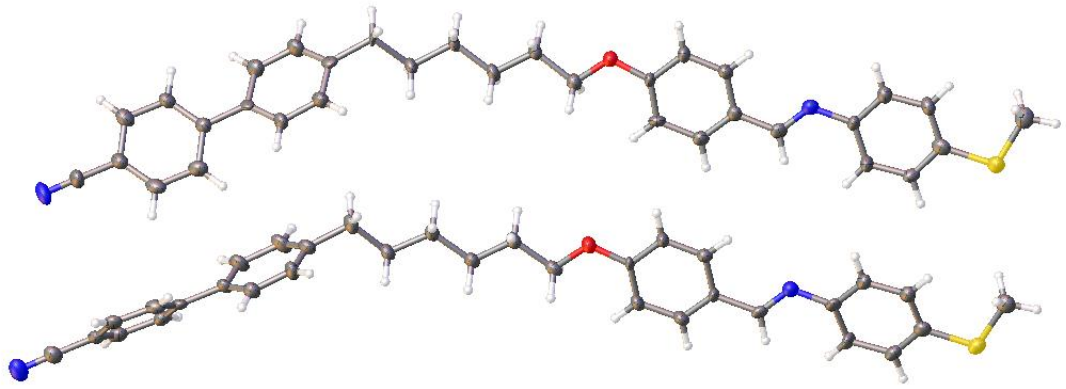

Figure S4 Two independent molecules of the CB6O.S1 in a single crystal. Atomic displacement parameters represented at 50% probability level.

There are 2 molecules in the asymmetric unit, and 4 molecules in the unit cell. The two independent molecules differ only in the biphenyl conformation – the difference facilitate formation of short C – H … π contacts between the biphenyl moieties, the shortest of them being C9 … H49 (2.722(7)Å) and C41 … H61 (2.718(8)Å). The alkyl linker in the dimer is fully stretched and in all *trans* conformation. Molecules align roughly along the [101] (**ac)** lattice diagonal, but do not form well defined layers.

Hirshfeld Surface analysis[14] as implemented in CrystalExplorer17[15] has been used to ascertain which intermolecular interactions are the most important or and the most common in the crystal structures of **CB6O.S1** and **CB6O.S2**. Based on the assumed structural and electron density model the approach defines a perimeter – a Hirshfeld Surface (HS) enclosing a molecule and containing the space where the contribution of this particular molecule to the total electron density exceeds 50%. All interatomic contacts between the molecule and its surrounding can then be mapped on such a surface, and color-coded: red if the interatomic contacts are shorter than the sum of atomic van der Waals radii or blue, if they are longer than such sum. The former indicate a stabilizing intermolecular interaction. In addition, a total percentage of certain interatomic contacts across HS can be presented, indicating the prevalent kind of intermolecular interactions.
In the case of **CB6O.S1** main intermolecular interactions involve:

C – H … π interactions between the biphenyl moieties of the adjacent molecules
(C...H contacts, 29% of all intermolecular contacts)
C – H … N interactions from aliphatic CH2 toward the terminal – CN group
C – H … N interactions from aromatic C – H toward the imide N
(N...H contacts, 10% of all intermolecular contacts)
C – H … S interactions involving the thioether group
(S...H contacts, 3.6% of all intermolecular contacts)
C – H … O interactions from phenyl C – H toward the ether O
(O...H contacts, 1.9% of all intermolecular contacts)
No π … π stacking interactions, or direct S … S contacts, which would be indicated by S...S or C...C short contacts across the HS, were detected.

Crystal packing maximizes the amount of C – H … S interactions involving the thioether group and C – H … N interactions from aliphatic CH_2 toward the terminal – CN group.

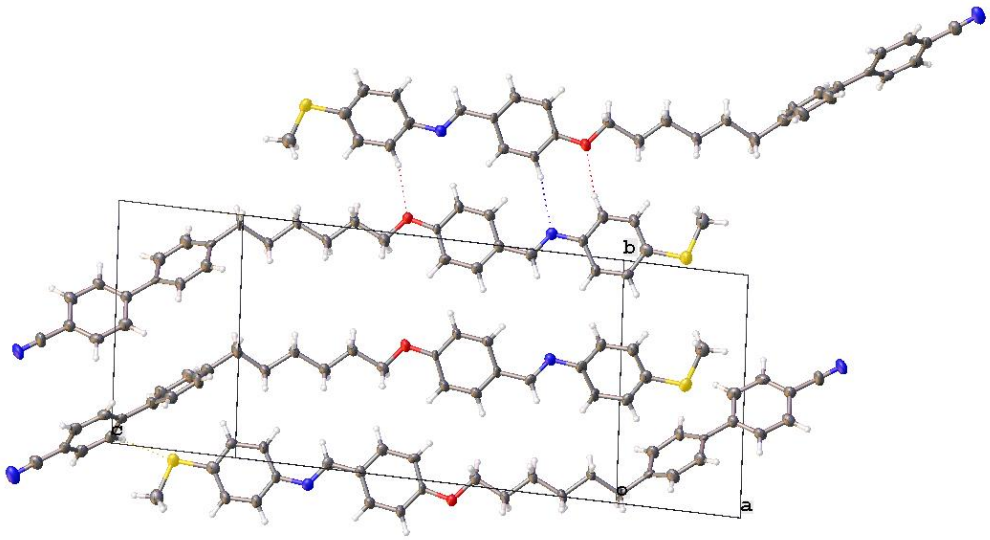

Figure S5 Illustration of main molecular interactions in CB6O.S_1 homologue

CB6O.S2

(a)

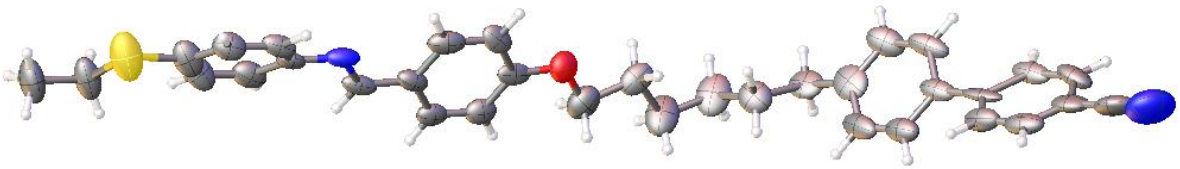

(b)

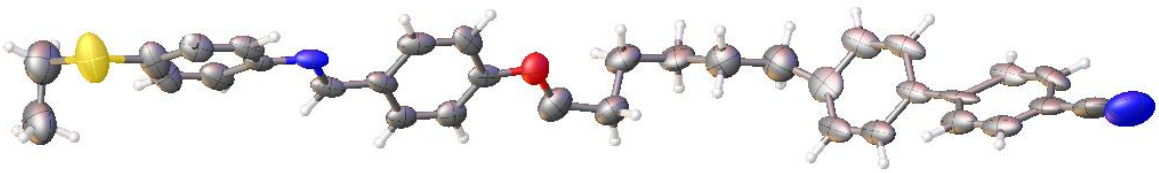

Figure S6 Alternative conformations of an independent CB6O.S2 molecule in a single crystal. Atomic displacement parameters represented at 50% probability level.

There is 1 molecule in the asymmetric unit and 4 molecules in the unit cell.

The molecule displays at least 2 alternative conformations which affect the C6 linker and the terminal –S–Et group. In both conformers the C6 linker is not fully stretched. The conformation of the linker is responsible for kinked shape of the molecules in the crystal structure. The **c** lattice constant approximates the molecule's length. The shortest intermolecular contacts are again C – H … π interactions, the shortest of them being C27 … H30 (2.641(8)Å) and C23 … H6 (2.786(7)Å)

In the case of **CB6O.S2** main intermolecular interactions involve:
C – H … π interactions between the biphenyl moieties of the adjacent molecules
(C...H contacts, 32.2% of all intermolecular contacts)
C – H … N interactions toward the terminal – CN group and the imide N
(N...H contacts, 10.0% of all intermolecular contacts)
C – H … S interactions involving the thioether group
(S...H contacts, 3.5% of all intermolecular contacts)
C – H … O interactions from phenyl C – H and linker CH2 towards the ether O
(O...H contacts, 2.6% of all intermolecular contacts)

Adjacent molecules form a layer in **a** direction, stabilized by the C – H … π interactions of the phenyl moieties. Consecutive layers in **b** direction are shifted by ½ **c**. The molecules are arranged so that the kink introduced by thioether group in one layer overlays the kink in the C6 linker of the next layer. As a result, the thioether S is surrounded by the aliphatic linkers of the adjacent molecules, forming a number of C – H … S short contacts.

Similarly to **CB6O.S1** no π … π stacking interactions or direct S … S contacts were detected. The according short S...S or C...C contacts across the HS were totally absent (0% of all interactions).

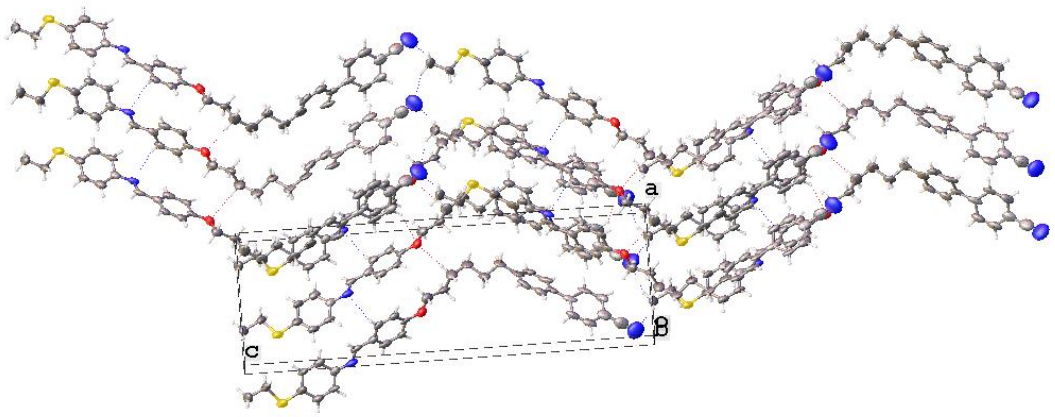

Figure S7 Illustration of main molecular interactions in CB6O.S2 homologue

S3. Temperature dependence of elastic constants

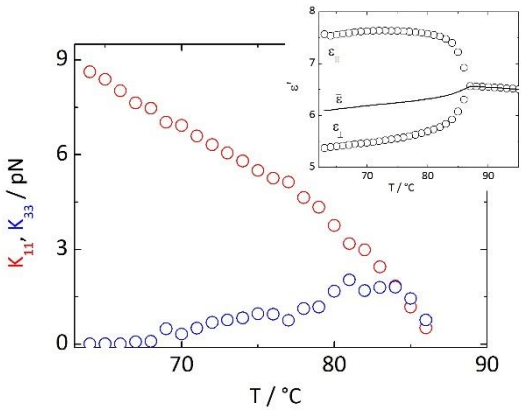

Figure S8. Temperature dependence of the splay (K_{11}, red circles) and bend (K_{33}, blue circles) elastic constants in the nematic phase of CB6O.S9. In the inset, the static dielectric permittivity as a function of temperature.

S4. B4 phase thermodynamic characterization – DSC

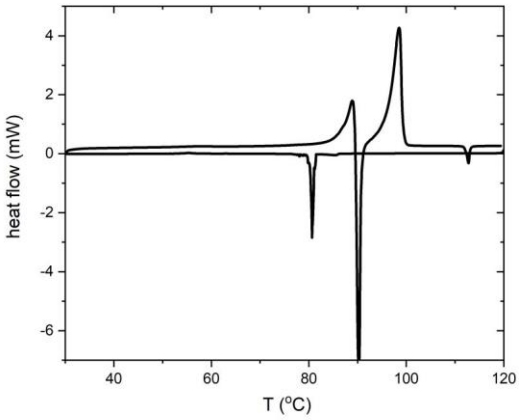

Figure S9 In calorimetric measurements the B4 phase was observed regardless of applied cooling rate, rapid cooling was necessary only in case of samples in glass cells. Formation of B4 crystal was accompanied by enthalpy change of the order of 50 kJ/mol. Interestingly, when heated B4 phase was transformed exothermally into another crystalline form.

S5. References

1. Abberley, J. P., Killah, R., Walker, R., Storey, J. M. D., Imrie, C. T., Salamończyk, M., Zhu, C., Gorecka, E. & Pociecha, D. Heliconical smectic phases formed by achiral molecules. *Nat. Commun.* **9**, 228 (2018).
2. Arakawa, Y., Komatsu, K., Inui, S. & Tsuji, H. Thioether-linked liquid crystal dimers

and trimers: The twist-bend nematic phase. *J. Mol. Struct.* **1199**, 126913 (2020).

3. Walker, R., Pociecha, D., Strachan, G. J., Storey, J. M. D., Gorecka, E. & Imrie, C. T. Molecular curvature, specific intermolecular interactions and the twist-bend nematic phase: the synthesis and characterisation of the 1-(4-cyanobiphenyl-4′-yl)-6-(4-alkylanilinebenzylidene-4′-oxy)hexanes (CB6O.*m*). *Soft Matter*. **15**, 3188–3197 (2019).
4. Quan, Z. J., Ren, R. G., Da, Y. X., Zhang, Z. & Wang, X. C. Alkylation of SH-heterocycles with Diethyl Phosphite using Tetrachloroethylene as an Efficient Solvent. *Heteroat. Chem.* **22**, 653–658 (2011).
5. Acosta-Guzmán, P., Mahecha-Mahecha, C. & Gamba-Sánchez, D. Electrophilic Chlorine from Chlorosulfonium Salts: A Highly Chemoselective Reduction of Sulfoxides. *Chem. – A Eur. J.* **26**, 10348–10354 (2020).
6. Duan, Z., Ranjit, S. & Liu, X. One-pot synthesis of amine-substituted aryl sulfides and benzo[b]thiophene derivatives. *Org. Lett.* **12**, 2430–2433 (2010).
7. Videnović, M., Mojsin, M., Stevanović, M., Opsenica, I., Srdić-Rajić, T. & Šolaja, B. Benzothiazole carbamates and amides as antiproliferative species. *Eur. J. Med. Chem.* **157**, 1096–1114 (2018).
8. Braunerová, G., Buchta, V., Silva, L., Kuneš, J. & Palát, K. Synthesis and in vitro antifungal activity of 4-substituted phenylguanidinium salts. *Farmaco*. **59**, 443–450 (2004).
9. Xu, J., Liu, R. Y., Yeung, C. S. & Buchwald, S. L. Monophosphine Ligands Promote Pd-Catalyzed C-S Cross-Coupling Reactions at Room Temperature with Soluble Bases. ACS Catal. 9, 6461–6466 (2019).
10. CrysAlisPro 1.171.38.43d (Rigaku OD, 2015)
11. G. Sheldrick, A short history of SHELX, Acta Crystallographica Section A, 64 (2008) 112-122.
12. G. Sheldrick, Acta Crystallographica Section C, 71 (2015) 3-8
13. O.V. Dolomanov, L.J. Bourhis, R.J. Gildea, J.A.K. Howard, H. Puschmann, OLEX2: a complete structure solution, refinement and analysis program, Journal of Applied Crystallography, 42 (2009) 339-341.
14. M. A. Spackman, D. Jayatilaka, CrystEngComm, 2009,11,19-32
15. C. F. Mackenzie, P. R. Spackman, D. Jayatilaka, M. A. Spackman, IUCrJ. 2017 4(5), 575-587.